Activity-dependent FosB gene expression negatively regulates mast cell functions.

Natalia Duque-Wilckens[1,2,3], Nidia Maradiaga[2], Yeh Szu-Ying[4], Dimitry Joseph[1], Vidhula Srinavasan[1], Kyan Thelen[2], Fabiola Sotomayor[1], Kait Durga[1], Eric Nestler[4], Adam J Moeser[2]*, A.J. Robison[1]*

[1]Department of Physiology, Michigan State University, East Lansing, MI, USA

[2]Department of Large Animal Clinical Sciences, Michigan State University, East Lansing, MI, USA

[3]Department of Biological Sciences, North Carolina State University, Raleigh, NC, USA

[4]Nash Family Department of Neuroscience and Friedman Brain Institute, Icahn School of Medicine at Mount Sinai, New York, New York

*Co-corresponding authors

Direct correspondence to:

AJ Robison: robiso45@msu.edu

Adam Moeser: moeserad@msu.edu

Abstract

Mast cells are innate immune cells that play a crucial role in numerous physiological processes across tissues by releasing pre-stored and newly synthesized mediators in response to stimuli, an activity largely driven by changes in gene expression. Given their widespread influence, dysfunction in mast cells can contribute to a variety of pathologies including allergies, long COVID, and autoimmune and neuroinflammatory disorders. Despite this, the specific transcriptional mechanisms that control mast cell mediator release remain poorly understood, significantly hindering the development of effective therapeutic strategies. We found that the two proteins encoded by the transcription factor FosB, FOSB and the highly stable variant ΔFOSB, are robustly expressed upon stimulation in both murine and human mast cell progenitors. Motivated by these findings, we generated a novel mouse model with targeted ablation of FosB gene expression specifically in mast cells (MC^{FosB-}) by crossing a mast cell-specific Cre reporter line (Mcpt5-Cre) with a Cre-dependent floxed FosB mouse lines. We found that mast cell progenitors derived from MC^{FosB-} mice, compared to wild types (WT), exhibit baseline increased histamine content and vesicle numbers. Additionally, they show enhanced calcium mobilization, degranulation, and histamine release following allergy-related IgE-mediated stimulation, along with heightened IL-6 release in response to infection-like LPS stimulation. *In vivo* experiments with IgE-mediated and LPS challenges revealed that MC^{FosB-} mice experience greater drops in body temperature, heightened activation of tissue-resident mast cells, and increased release of pro-inflammatory mediators compared to their WT counterparts. These findings suggest that FosB products play a crucial regulatory role in moderating stimulus-induced mast cell activation in response to both IgE and LPS stimuli. Lastly, by integrating CUT&RUN and RNAseq data, we identified several genes targeted by ΔFOSB that could mediate these observed effects, including Mir155hg, CLCF1, DUSP4, and Trib1. Together, this study provides the first evidence that FOSB/ΔFOSB modulate mast cell functions and provides a new possible target for therapeutic interventions aimed at ameliorating mast cell-related diseases.

Graphical Abstract

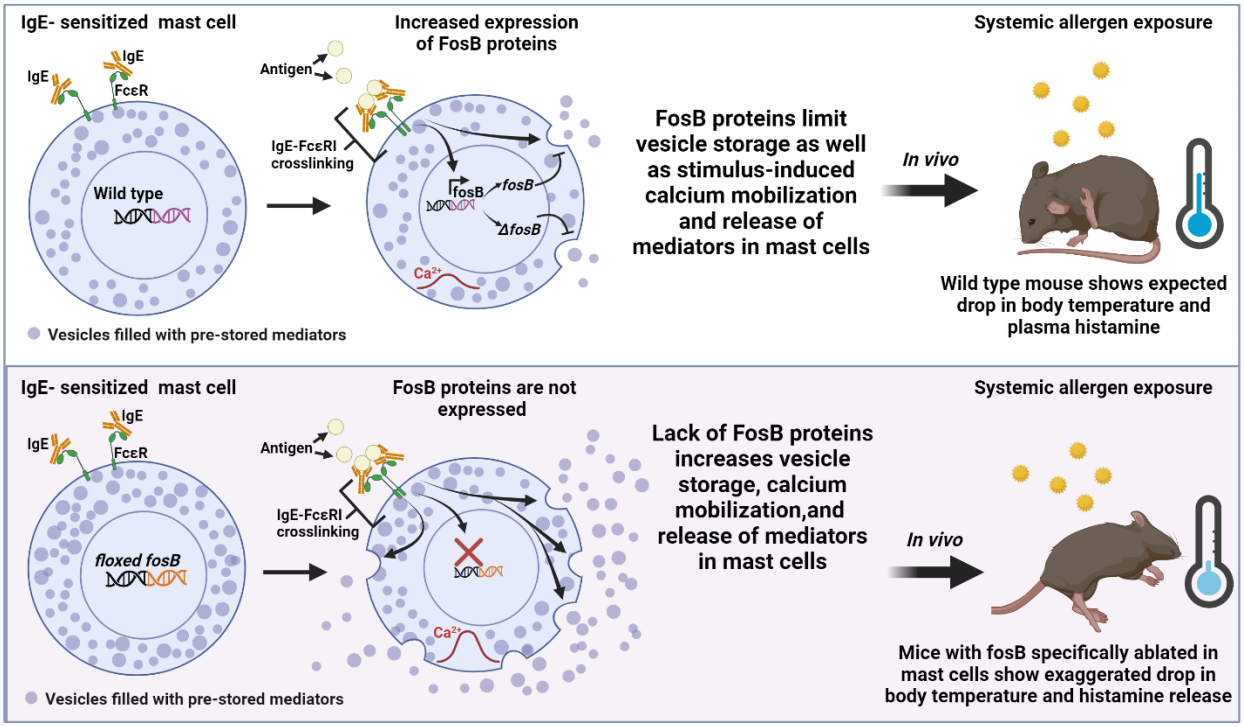

Introduction

Mast cells, highly conserved components of the innate immune system, play a pivotal role in myriad physiological and pathological processes. They are ubiquitously present across tissues, especially near surface areas like skin and close to blood and lymph vessels[1,2]. Furthermore, their ability to express a vast array of receptors enables them to respond to a wide range of stimuli, including signals from pathogens and cellular damage[3], environmental toxins and contaminants[4,5], immune cells[6,7] and signaling molecules[8–10], neurotransmitters and neuropeptides[11,12], as well as various hormones associated with stress responses[13,14], metabolism[15,16], sexual development[17,18], and circadian rhythms[19]. Critically, upon activation, mast cells can release a variety of both preformed and newly synthesized mediators ranging from immune signaling molecules such as chemokines and cytokines[20], to lipid mediators like prostaglandins and leukotrienes[21], and neurotransmitters such as serotonin[22], histamine[23], and dopamine[24], along with ATP[25] and growth factors such as VEGF[26] and NGF[27]. Consequently, mast cells are strategically positioned to act as body-wide sentinels, initiating, modulating, and amplifying multicellular responses to internal and external stimuli.

Given their many crucial roles, dysregulation of mast cell functions contributes to the pathology of numerous diseases. For example, mast cell dysfunction is central to disorders such as pathological allergies[28], migraines[29,30], inflammatory bowel disease[31,32], multiple sclerosis[33], and rheumatoid arthritis[34]. Additionally, accumulating data suggest that mast cells play important roles in cancer[35,36], long COVID[37], chemical intolerance[38], and chronic neurological and neurodegenerative diseases such as autism[39] and Alzheimer's[40]. Therefore, identifying the regulatory mechanisms underlying gene expression and activity that drive mast cell involvement in physiology and disease is crucial for developing strategies to both enhance their protective functions and mitigate their adverse impacts across systems.

In an RNAseq screen designed to investigate gene regulation in mouse bone marrow-derived mast cells (BMMCs) following IgE-FcεRI crosslinking—a key mechanism of mast cell activation during allergic inflammation[41]—we found that FosB was one of the genes most robustly upregulated. FosB has been extensively characterized in neurons as an immediate

early gene that, through alternative splicing, encodes two primary proteins: FOSB and ΔFOSB. Both proteins can form heterodimers with Jun family proteins to create activator protein-1 (AP-1) transcription factor complexes to regulate gene expression across multiple signaling pathways and functional outcomes[42–45]. While FOSB, like other proteins of the Fos family, is degraded within hours after induction, ΔFOSB is remarkably stable. In neurons, this stability is a critical mechanism by which ΔFOSB exerts long-term modulation of gene expression after chronic exposure to stress[42,46,47] or drugs of abuse[48], as well as in memory formation[49]. Intriguingly, the FosB gene was also among the most strongly upregulated genes in a different study where BMMCs were stimulated with glutamate[12], a neurotransmitter linked to neuron-mast cell communication in response to tissue injury. Together, these findings suggest that FosB may serve as a central mechanism modulating diverse pathways of mast cell activation.

Motivated by these findings, we aimed to dissect FosB's specific functions in mast cells. We generated a novel mouse model by crossing a mast cell-specific Cre reporter, Mcpt5-Cre[50], with a Cre-dependent floxed FosB[51] mouse line. This resulted in the first mice with targeted ablation of FosB gene expression specifically in mast cells (MC^{FosB-}). Next, using a combination of *in vitro* and *in vivo* approaches, we found that FosB plays a regulatory role in limiting stimulus-induced mast cell activation and allergy- and infection-related physiological responses. Furthermore, by employing Cleavage Under Targets and Release Using Nuclease (CUT&RUN), we were able to provide a comprehensive mapping of genomic regions targeted by ΔFOSB in both unstimulated and stimulated BMMCs. Our findings indicate that ΔFOSB in mast cells binds to multiple distinct genes, varying significantly between unstimulated and stimulated states. Interestingly, most of these binding sites are located outside of known promoter regions, predominantly within distal intergenic regions or gene bodies, reflecting similar findings recently observed in neurons[52]. Lastly, by integrating CUT&RUN with previously obtained RNAseq data from both unstimulated and stimulated IgE-sensitized BMMCs, we identified multiple differentially expressed genes as potential functional targets of ΔFOSB in the context of IgE-FcεRI crosslinking. These targets, which include Mir155hg, CLCF1, DUSP4, and Trib1, could potentially play key roles in modulating mast cell mediator

release and could be explored as focal points for therapeutic intervention. Altogether, these findings reveal that FosB serves as a critical regulator in diverse mast cell activation pathways relevant to allergy and infection.

Results

1. IgE-mediated and LPS stimulations increase fosB gene expression in mast cells progenitors.

Building on our initial RNA screening results, which identified FosB as one of the most upregulated genes following IgE-FcεRI crosslinking, we aimed to validate this finding and extend our research to additional mast cell activation mechanisms. Consequently, we employed qPCR and western blot to examine FosB expression in response to two distinct pathways of mast cell activation: allergy-related IgE-mediated FcεRI crosslinking and infection-like lipopolysaccharide (LPS) stimulation.

IgE-mediated FcεRI cross-linking is one of the most extensively studied pathways underlying the involvement of mast cells in allergic inflammation[41]. At a cellular level, this process begins with the binding of IgE antibodies to the high-affinity receptor FcεRI on mast cell surfaces. When IgE-sensitized mast cells contact the antigen, IgE-FcεRI complexes cross-link, triggering downstream signaling cascades. These cascades lead to the rapid mobilization of calcium (Ca^{2+}) and the release of preformed mediators stored in cytoplasmic granules (such as vasoactive amines and proteases), as well as the *de novo* synthesis of proinflammatory lipid mediators, cytokines, and chemokines[53,54]. To test the effects of IgE-mediated FcεRI cross-linking on fosB expression, we sensitized BMMCs overnight with 0.8 µg/ml IgE anti-2,4-dinitrophenyl (DNP), and then challenged sensitized BMMCs with 15.5 ng/ml DNP (**fig.1A**), as previously described[55,56]. We found that in sensitized BMMCs, exposure to DNP vs. vehicle significantly increased the expression of both *fosB* (**fig. 1C,** one-tailed T-test $t_{(4)}=8.96$, $p=0.0004$, $R^2=0.95$) and *ΔfosB* (**fig. 1D**, one-tailed t-test $t_{(4)}=13.50$, $p<0.0001$, $R^2=0.97$) mRNAs. Western blot analyses (**fig. 1B**) further showed that this was true at the protein level for both FOSB (**fig. 1E,** one-tailed T-test $t_{(4)}=2.411$, $p=0.004$, $R^2=0.59$) and

ΔFOSB (**fig. 1F,** one-tailed T-test $t_{(4)}$=2.28, p=0.04, R^2=0.56). To our knowledge, this is the first time that *ΔFosB* expression has been demonstrated in mast cells.

In addition to their well-known role in allergic responses, mast cells play a key role in the immune defense against several pathogens. They do so by expressing a wide variety of receptors, including the Toll-like family of receptors (TLR)[3,57], which recognize pathogen-associated molecules. TLR-mediated activation does not result in Ca^{2+} mobilization or mast cell degranulation[58,59], but it initiates the selective synthesis and release of cytokines and chemokines, which in turn recruit other immune cells to the site of invasion[58,60,61]. To test whether FosB is involved in TLR-mediated mast cell responses, we next stimulated BMMCs with 1mg/ml LPS (**Fig. 1G**), a component of gram-negative bacteria[62] that is recognized by mast cells through TLR4[61]. LPS stimulation also upregulated both *fosB* (**fig. 1H,** one-tailed T-test $t_{(4)}$=2.2, p=0.046, R^2=0.54) and *ΔfosB* (**fig. 1I**, one-tailed t-test $t_{(4)}$=5.47, p=0.002, R^2=0.88).

Lastly, to test whether FosB is expressed in human mast cells, we did western blot analyses on the LAD2 human mast cell line[63] stimulated with compound 48/80 (a generous donation by A. Kirshenbaum, NIH, USA) , which triggers IgE-independent mast cell degranulation by targeting the orphan receptor Mas-related G protein-coupled receptor-B2 (Mrgprb2)[64]. We found clear bands at the ~50KdA and ~37kDA (**fig. 1J**) confirming the presence of both FosB and ΔFosB, respectively, in activated human-derived mast cells.

These findings, together with previous reports that stimulation with glutamate (via binding to ionotropic and metabotropic glutamate receptors on the mast cell surface)[65] or cholesterol (by modulating the organization of lipid rafts)[66] also upregulate FosB expression in mast cells, suggest that FosB-derived proteins may be a key modulator of mast cell activation across diverse signaling pathways. To further investigate the function of FOSB/ΔFOSB in mast cells, we crossed Mcpt5-Cre[50] mice with Cre-dependent floxed FosB[51] mice, creating the first mice in which FosB gene expression is ablated specifically in MCs (MC^{FosB-}).

2. Inhibition of FosB gene expression in mast cells enhances storage capacity, increases sensitivity and histamine release in response to IgE-FcεRI crosslinking, and augments IL-6 release in response to LPS stimulation.

After confirming mast cell purity by co-expression of ckit and FcεRI in both WT and MC^{FosB-} derived BMMCs (supplementary figure 1A), we assessed FosB gene expression in MC^{FosB-} by testing unstimulated and stimulated BMMCs derived from WT and MC^{FosB-} mice (**fig. 2A**). Consistent with our initial findings, DNP increased *fosB* (**fig. 2B**, two-way ANOVA treatment $F_{(1, 8)} = 4.5$, p=0.06, Fisher's LSD WT IgE-Veh vs. IgE-DNP p=0.02) and *ΔfosB* mRNA (**fig. 2C**, two-way ANOVA treatment $F_{(1, 8)} = 4.8$, p=0.06, Fisher's LSD WT IgE-Veh vs. IgE-DNP p=0.02) in WT BMMCs. However, expression in both unstimulated and stimulated MC^{FosB-} BMMCs was minimal. Western blot analyses further confirmed that, unlike WT, MC^{FosB-} BMMCs showed no expression of FOSB or ΔFOSB protein either at baseline or after DNP stimulation (**fig. 2D**). Together, this confirms that the FosB gene is effectively inhibited in BMMCs derived from MC^{FosB-} mice.

Next, we explored the impact of inhibiting FosB expression on the release of histamine, one of the predominant bioactive amines stored in mast cell granules and extensively released in response to IgE-FcεRI crosslinking[23]. We found that DNP stimulation induced significantly higher histamine release in MC^{FosB-} BMMCs vs WT BMMCs (**fig. 2E**, two-way ANOVA interaction $F_{(1, 8)} = 9.9$, p=0.01, Fisher's LSD DNP WT vs MC^{FosB-} p=0.002, R^2=0.72; vehicle WT vs MC^{FosB-} *ns*). To determine whether this increased histamine release could be attributed to either an elevated basal content of histamine or heightened sensitivity to activation in MC^{FosB-} BMMCs, we measured both the basal histamine content and stimulus-induced intracellular Ca^{2+} mobilization, a key event needed for mast cell degranulation[67]. ELISA analyses showed that MC^{FosB-}, compared to WT, had significantly higher content of histamine (**fig. 2F**, one-tailed T-test $t_{(4)}$=3.642, p=0.01, R^2=0.76), suggesting that, at baseline, FOSB/ΔFOSB may be involved in limiting mast cell storage capacity. Interestingly, Ca^{2+} mobilization studies in IgE-sensitized WT and MC^{FosB-} BMMCs showed that DNP elicited a significantly higher fluorescence ratio in MC^{FosB-} compared to WT (**fig. 2G,** repeated measures two-way ANOVA genotype x time interaction effect $F_{(999, 13986)}$=3.597 p <0.0001,

AUC between seconds 50 and 200 one-tailed T-test $t_{(14)}$=3.5, p=0.002, R^2=0.46), suggesting that MC^{FosB-} mast cells are more sensitive to activation. To further investigate whether the heightened sensitivity to activation in MC^{FosB-} mast cells is upstream or downstream of FcεRI activation, we stimulated WT and MC^{FosB-} BMMCs with 0.1 mM A23187, a Ca^{2+} ionophore. A23187 directly activates membrane Ca^{2+} channels and induces Ca^{2+} release from endoplasmic reticulum stores[68], bypassing the need for FcεRI activation. We found that A23187 also induced a sustainably higher intracellular Ca^{2+} mobilization in MC^{FosB-} vs. WT (**fig. 2H**, repeated measures two-way ANOVA genotype x time interaction effect $F_{(999, 13986)}$=6.6 p <0.0001, AUC between seconds 50 and 200 one-tailed T-test $t_{(14)}$=1.96, p=0.03 R^2=0.21). Together, these data suggest that FosB-derived proteins act downstream of FcεRI to limit mast cell activation.

Lastly, we examined whether inhibition of FosB gene expression would affect mast cells at the ultrastructural level. For this, we used transmission electron microscopy (TEM) [69,70] of IgE-sensitized WT and MC^{FosB-} BMMCs after vehicle or DNP stimulation. Quantitative assessment was performed by a blind observer, focusing on vesicle number (**fig 2K**, vesicles indicated by yellow arrows) and the degree of degranulation based on content of electron dense granules within the vesicles (**fig. 2M**, highly degranulated mast cells-mostly empty vesicles- indicated by red arrows and minimally degranulated mast cells indicated by green arrows). While MC^{FosB-} BMMCs showed a "typical" mast cell phenotype (i.e. large nucleus and multiple vesicles filled with electron-dense granules), compared to WT, MC^{FosB-} BMMC showed significantly elevated vesicle number (**fig. 2J,** one-tailed T-test $t_{(4)}$=3.6, p=0.01, R^2=0.76), suggesting that the elevated histamine content in MC^{FosB-} could be at least partly due to an increased storage capacity. Further, DNP stimulated MC^{FosB-} vs WT BMMCs showed an increased ratio of highly degranulated vs. total mast cells (**fig. 2L,** two-way ANOVA interaction $F_{(1, 76)}$=12.9, p=0.0006, Fisher's LSD veh vs DNP MC^{FosB-} p<0.0001, R^2=0.48; veh vs DNP WT *ns*), further supporting that MC^{FosB-} BMMCs show heightened sensitivity to stimulus-induced activation.

Finally, based on the initial finding that LPS stimulation also upregulates *fosB/ΔfosB* expression, we measured LPS-induced release of the inflammatory cytokine interleukin-6

(IL-6) at baseline, 6 and 24h after stimulation. We found that, while both WT and MC^{FosB-} BMMCs release IL-6 in response to LPS stimulation in a time-dependent manner (**fig. 2I,** two-way ANOVA main effect of time $F_{(2,11)}$=6.195 p=0.01), only MC^{FosB-} show a significant increase between baseline and 24h (Fisher's LSD baseline vs. LPS 24h WT p=0.01, R^2=0.57; baseline vs. LPS 24h MC^{FosB-} *ns*), suggesting that FosB gene expression may also play a role in limiting the TLR-4 mediated *de novo* synthesis of inflammatory cytokines[62].

Together, these findings suggest that FosB-derived proteins play a crucial role in moderating the activation of BMMCs by regulating pathways involved in vesicle biogenesis and/or trafficking, intracellular Ca^{2+} mobilization, and the storage and synthesis of mediators. To determine the relevance of these findings *in vivo*, we next evaluated the physiological and cellular responses to systemic IgE-FcεRI and TLR-4 stimulations in WT and MC^{FosB-} mice.

3. Mast cell-specific knockout of FosB exacerbates inflammatory responses in models of systemic anaphylaxis and lipopolysaccharide-induced sepsis

We initially investigated whether there were any basal phenotypic differences between MC^{FosB-} and WT mice. Our observations revealed no differences in body weight at 6 weeks of age (**Fig. 3B**), number of mast cells detected in mesenteric tissue (**Fig. 3C**), or locomotor activity as measured by the total distance traveled (**Fig. 3D**) or velocity (**Fig. 3E**) in the open field test.

Next, we used the mast cell-dependent model of IgE-mediated passive systemic anaphylaxis (PSA) to evaluate *in vivo* IgE-FcεRI-dependent mast cell activity. WT and MC^{FosB-} mice were sensitized with an i.p. injection of 5 µg anti-DNP IgE monoclonal antibody and then challenged the following day with 50 µg DNP administered i.p. to induce anaphylaxis, as previously described[69] (**fig. 3F**). Rectal temperature was measured every 5 minutes following DNP administration to assess PSA-induced hypothermia, a mast cell-dependent response[71]. 25 minutes after DNP stimulation, mice were euthanized, and blood as well as intestinal mesentery were collected for the assessment of plasma histamine and mast cell histology, respectively. We found a significant interaction between time and genotype in

rectal temperature measures (**fig. 3G**, repeated measures two-way ANOVA time x genotype interaction $F_{(5,100)}$ =5.96, p<0.0001). Compared with WT, MC^{FosB-} mice showed an exaggerated peak drop in rectal temperature (Fisher's LSD multiple comparisons WT vs MC^{FosB-} at min 25 p=0.01 R^2=0.2471, Δ body temp= -3.7±2.0°C vs. -5.6±1.4°C in WT and MC^{FosB-} mice, respectively), significantly higher plasma histamine (**fig. 3H,** one-tailed T-test $t_{(20)}$= 2.415, p=0.01, R^2=0.22), and an increased ratio of active (degranulating) vs. inactive (non-degranulating) mesentery mast cells (**fig. 3I,** one-tailed T-test $t_{(8)}$= 2.65, p=0.01, R^2=0.46).

Finally, we stimulated WT vs MC^{FosB-} mice with a 1 mg/Kg LPS IP and measured rectal temperature every 60 min for 6h (**fig.3J**). This high dose of LPS, as opposed to a lower dose, induces mast cell-dependent hypothermia[72], a response typical of more severe cases of sepsis[73]. Similar to PSA, there was a significant interaction between time and genotype in rectal temperature measures (**fig. 3K**, repeated measures two-way ANOVA time x genotype interaction $F_{(6,84)}$=3.32, p<0.006). Compared with WT, MC^{FosB-} mice showed an exaggerated drop in rectal temperature (Fisher's LSD multiple comparisons WT vs MC^{FosB-} at hour 6 p=0.02, R^2=0.35, Δ body temp= -1.7±1.3°C vs. -3.9±1.8°C in WT and MC^{FosB-} mice, respectively), and a trend for higher clinical scores at min 360 (**supplementary fig. 2A**, repeated measures two-way ANOVA main effect of time, Fisher's LSD WT vs MC^{FosB-} at min 360 p=0.08) and a trend for elevated plasma concentration of IL-6 (**fig. 3L,** one tailed T-test $t_{(5)}$=1.638, p=0.08, R^2=0.35) as well as active vs. inactive mast cells (**fig. 3M,** one tailed T-test $t_{(8)}$=1.8, p=0.05, R^2=0.29). Finally, based on recent findings that LPS-induced neuroinflammation, which results in increased anxiety-like behaviors[74,75], is mediated by mast cells[76,77], in a separate cohort we tested WT and MC^{FosB-} mice in the elevated plus maze 24h post-LPS or vehicle administration. We found a main effect of treatment on the time spent in the open vs. closed arms (**fig. 3N**, two-way ANOVA main effect of treatment $F_{(1,24)}$=6.62, p=0.01). Interestingly, this effect was stronger in MC^{FosB-} mice (Fisher's LSD vehicle vs. LPS MC^{FosB-} p=0.04, R^2=0.39; vehicle vs. LPS WT *ns*, R^2=0.11,), suggesting that LPS induces a stronger neuroinflammatory response in MC^{FosB-} mice compared to WT. Consistent with these findings, we found a stronger expression of *tnf alpha* mRNA in hypothalamus from LPS-treated MC^{FosB-} vs. WT mice (**supplementary fig. 2B**).

Together, these results suggest that FosB plays a regulatory role in limiting stimulus-induced mast cell activation *in vivo*, consistent with *in vitro* findings. To further elucidate the underlying molecular mechanisms, we conducted Cleavage Under Targets and Release Using Nuclease (CUT&RUN)[78] profiling to detect genome-wide binding of ΔFOSB in IgE-sensitized WT BMMCs exposed to vehicle (unstimulated) or DNP (stimulated) (**fig.4A**).

4. Mapping binding sites of ΔFOSB in unstimulated and stimulated mast cells using CUT&RUN approach

Peaks obtained by CUT&RUN were first identified using Model-based Analysis of ChIP-Seq (MACS2)[79] and Irreproducible Discovery Rate (IDR)[80] on aligned sequencing data. MACS2 served as the primary peak calling module, while IDR was used to filter for consistent peaks across samples. 8,664 and 14,228 peaks were identified in stimulated and unstimulated WT BMMCs, respectively, with an additional 6,468 peaks shared between both conditions (**fig 4B**). Subsequent motif analysis of the peaks from both sample types using Multiple Em for Motif Elicitation (MEME)[81] revealed that AP-1 sites - the canonical binding response elements for FOS family proteins complexed with JUN family proteins - were present in over 98% of ΔFOSB peaks in unstimulated (8520 out of 8664, E-value 1.3×10^{-70}), and more than 99% in stimulated (14147 out of 14228, E-value 8.7×10^{-51}) WT BMMCs (**Fig. 4C**). To assess whether the peaks identified by ΔFOSB CUT&RUN are indeed genuine ΔFOSB binding sites, we used deepTools[82] to visualize the coverage of ΔFosB at these peak regions in MC^{FosB-} BMMCs. We found that the coverage in MC^{FosB-} BMMCs was dramatically reduced (**supplementary fig. 2C**). Next, to further confirm specificity, we used Pearson correlation coefficient to compare the coverage of ΔFosB at peaks in WT stimulated, WT unstimulated, MC^{FosB-} stimulated, and MC^{FosB-} unstimulated BMMCs (**supplementary fig. 2D**). The comparisons involving MC^{FosB-} BMMCs revealed a reduced correlation compared to WT BMMCs (WT stimulated vs unstimulated Pearson r= 0.76, WT stimulated vs MC^{FosB-} stimulated and unstimulated r=0.67 and r=0.45, respectively), suggesting that the peaks identified in WT samples are indeed specific to ΔFosB. However, the possibility of a minimal presence of WT cells in MC^{FosB-} samples cannot be entirely excluded, which may be a result

of incomplete Cre recombinase activity due to low expression of MCPT5 in some BMMCs in the MC^{FosB-} group.

Next, we identified genomic regions to which ΔFOSB binds under stimulated conditions by annotating the peaks based on their location in the mouse reference genome (mm10). About 15% of ΔFOSB peaks were found within putative promoter regions, i.e., <=1000 and +2000 bp of known transcription start sites. Around 28% of the peaks were located in intergenic regions, and roughly half of the peaks were found within gene bodies (**figure 4D**). Interestingly, this pattern for ΔFOSB to bind sites outside promoter regions was recently observed for ΔFOSB in mouse neurons[52].

Next, to elucidate the potential functional roles of ΔFosB-bound genomic regions, we employed HOMER[83] software to annotate each peak with its nearest gene, thereby linking DNA-binding events to potential gene regulatory functions. We generated two gene lists corresponding to the binding sites in both unstimulated and stimulated WT BMMCs (**supplementary tables 1 and 2**). These gene lists were then subjected to Gene Ontology (GO) term analysis with a focus on molecular function, using the Gene Ontology Consortium (http://geneontology.org/) for functional gene annotation. This analysis was performed through the PANTHER Classification System[84], employing Fisher's exact test ($p<0.05$) and applying false discovery rate (FDR) correction with a threshold of 0.05 for statistical significance.

The GO of genes associated with ΔFosB binding in IgE-Veh BMMCs (**fig. 4E for 41 genes with highest FDR supplementary table 3 for full list**) revealed several functional categories that are enriched. Notably, lipid metabolism is a prominent category, highlighted by genes involved in very-low-density lipoprotein (VLDL) particle receptor binding (GO:0030229), stearoyl-CoA 9-desaturase activity (GO:0004768), and acyl-CoA desaturase activity (GO:0016215). This finding is intriguing because lipid metabolism is crucial in mast cell functions, including the synthesis of lipid mediators, modulation of membrane fluidity, and regulation of signaling pathways associated with FcER and TLR activation[85–87]. In addition, inflammatory pathways also emerge as a significant category, with genes related to cytokine receptor activity (GO:0004896), chemokine receptor binding (GO:0042379), IL-6 receptor

binding (GO:0005138), and platelet-derived growth factor receptor binding (PDGF, GO:0005161) being enriched.

The GO analysis of genes associated with ΔFosB binding in IgE-DNP BMMCs reveals several key functional categories that are enriched (**fig. 4F for 41 genes with highest FDR supplementary table 4 for full list**), including the LPS immune receptor activity (GO:0042832), the calcium, potassium:sodium antiporter activity (GO:0008273), and the enrichment of genes associated with MAPK tyrosine phosphatase activity (GO:0033550).

To narrow down the list of ΔFosB functional gene targets in the context of IgE-FcεRI mast cell activation, we next combined these data with previously obtained RNAseq data from unstimulated and stimulated WT BMMCs.

5. Identification of ΔFOSB functional targets in IgE-FcER stimulation in mast cells

We first aimed to identify RNAseq peaks that are statistically enriched in stimulated vs. unstimulated WT BMMCs. For this, we carried out a differential analysis utilizing the DiffBind package (v3.2.7)[88]. DiffBind utilizes DESeq2 for normalizing read counts, which helps in pinpointing specific genomic intervals where ΔFosB binding differs between the two conditions. We considered regions with an absolute log2 fold change of at least 1 and an FDR less than 0.05 as significantly different. This analysis revealed over 4,000 peak regions with substantially increased ΔFosB binding following stimulation (**figs. 5 A,B**).

Next, to identify ΔFOSB's functional targets during IgE-FceR stimulation, we first created a consensus peak set from peaks consistent across both stimulated and unstimulated cells. We then quantified the overlap of reads in each consensus peak interval for each sample. DiffBind, along with DESeq2 read count normalization, was used to identify unique genomic intervals with significant differential binding between stimulated and unstimulated cells, adhering to the same thresholds for significance.

Finally, we compared these data with RNA sequencing reads from stimulated and unstimulated mast cells mapped to the mm10 genome (**fig. 5C**). Using DESeq2 for differential expression analysis and setting a conservative threshold of at least a 1.3 log2 fold change and an FDR less than 0.05 to ensure the robustness of our findings, we identified 35

genes with significantly differential expression (**fig. 5D, E; full list in supplementary table 5**). Many of these genes, such as Phxr4, Zfp703, Fhdc1, and Sema4b, have not yet been characterized. However, some, based on findings in other cell types, could potentially limit mast cell activation. These include CLCF1, DUSP4, and Trib1 (see Discussion section). Notably, one identified gene, microRNA encoding Mir155hg[89], was shown to reduce FcεRI-mediated degranulation and pro-inflammatory cytokine release in mast cells by increasing protein kinas B (Akt) phosphorylation. Because Akt is activated by the phosphoinositide-3-kinase (PI3K) pathway, this strongly suggests that Mir155hg limits mast cell degranulation by targeting PI3K[89]. Interestingly, PI3K pathway also plays a crucial role in mediating mast cell responses to LPS activation through TLR4[62], suggesting that ΔFOSB could modulate both IgE and LPS-mediated degranulation by upregulating Mir155hg. Future studies should explore this possibility.

Discussion

Mast cells play a crucial role in numerous physiological processes across tissues by releasing pre-stored and newly synthesized mediators in response to stimuli, an activity largely driven by changes in gene expression. Given their widespread influence, dysfunction in mast cells can lead to a broad range of pathologies across multiple organ systems. Despite this, the specific transcriptional mechanisms that control the release of these mediators remain poorly understood, significantly hindering the development of effective therapeutic strategies. It was recently demonstrated that FosB, an immediate-early gene that mediates stimulus-induced changes in gene expression and is crucial for functional adaptations in neurons[90] and microglia[43], is robustly upregulated in mast cells following glutamate stimulation[12]. This finding, coupled with our observations that the two primary proteins encoded by FosB—FOSB and its highly stable variant ΔFOSB—are robustly expressed in both murine and human mast cell progenitors, prompted us to generate a mast cell-specific FosB ablation mouse model (MC^{FosB-}) to further investigate the specific role of FosB in mast cell function. *In vitro* studies demonstrated that mast cell progenitors derived from MC^{FosB-} mice, compared to WT, exhibited increased histamine content and vesicle count

at baseline. Additionally, the MC^{FosB-} cells showed enhanced calcium mobilization, degranulation, and histamine release following allergy-related IgE-mediated stimulation, as well as elevated IL-6 release in response to infection-like LPS stimulation. Complementary *in vivo* experiments with IgE-mediated and LPS challenges revealed that MC^{FosB-} mice experienced greater drops in body temperature, heightened activation of tissue-resident mast cells, and increased release of pro-inflammatory mediators compared to their WT counterparts. These findings suggest that FosB products play a crucial regulatory role in moderating stimulus-induced mast cell activation in response to both IgE and LPS stimuli. Furthermore, by integrating CUT&RUN and RNAseq data, we identified several genes targeted by ΔFOSB that could mediate these observed effects, including Mir155hg, CLCF1, DUSP4, and Trib1. Together, this study provides the first evidence that FOSB/ΔFOSB modulate mast cell functions and provides a new possible target for therapeutic interventions aimed at ameliorating mast cell-related diseases.

Lack of FosB increases vesicle number, sensitivity to activation, and release of mediators in mast cell progenitors

Our results showed that, compared to WT, unstimulated MC^{FosB-} BMMCs exhibit elevated histamine levels and increased number of vesicles. This suggests that FosB in mast cells plays a crucial role in limiting histamine synthesis and vesicle formation, maturation, or storage under baseline conditions. Intriguingly, CUT&RUN analysis identified genes associated with ΔFOSB that may influence these processes. Among them, type I interferons (IFN-I), which have been used clinically in the treatment of mastocytosis due to their ability to limit mast cell mediator release[91], are of particular interest. Recent studies suggest that IFN-I's therapeutic effects may be mediated, at least in part, by limiting secretory granule formation and histamine storage[92]. Therefore, it is possible that ΔFOSB modulates the biogenesis of secretory granules and histamine storage by upregulating IFN-I expression.

Another ΔFOSB-bound gene potentially involved in limiting histamine storage is mitochondrial uncoupling protein 2 (UCP2), which inhibits histamine synthesis in mast cells by suppressing histidine decarboxylase[93], the key enzyme in the histamine biosynthesis

pathway. Given that mast cells are significant histamine sources in regions like the gastrointestinal tract[94] and brain[95,96]—where histamine plays crucial roles in modulating visceral nociception, gut motility, gastric acid production[97] as well as food intake and sleep-wake cycles[96,98], respectively—it would be interesting to explore whether reduced histamine storage in MC^{Fosb-} mice affects these physiological functions.

In addition to the differences in histamine storage and vesicle number at baseline conditions, we found that MC^{FosB-} BMMCs show increased calcium mobilization in response IgE-mediated and calcium ionophore A23187 stimulations, as well as increased release of histamine or IL-6 in response to IgE-mediated or LPS stimulations, respectively. This suggests that FosB also plays a role in preventing exaggerated stimulus-induced mast cell activation and release of mediators, possibly through modulation of shared pathways downstream of FcεRI and TLR. CUT&RUN data in combination with RNAseq revealed several genes that could be associated with these effects, including Mir155hg, CLCF1, DUSP4, Trib1, Zbtb32, and Gpr171.

Mir155hg is the only gene with known functions in mast cells: its expression limits IgE-mediated mast cell degranulation by targeting the PI3K pathway[89], which acts downstream of IgE-FcεRI crosslinking to catalyze the phosphorylation of phosphatidylinositol (4,5)-bisphosphate (PIP2) into phosphatidylinositol (3,4,5)-trisphosphate (PIP3). PIP3, in turn, activates downstream signaling molecules such as Akt (Protein Kinase B), initiating a cascade that leads to mast cell degranulation[99]. Therefore, by increasing expression of Mir155hg, ΔFOSB could provide a mechanism that mitigates excessive mast cell degranulation in response to IgE-mediated stimulation. Interestingly, inhibition of the PI3K pathway in mast cells was also shown to reduce LPS-induced release of TNFα and IL-6[100,101]. Although we did not assess ΔFOSB binding in the context of LPS stimulation, it is possible that the exaggerated release of IL-6 in LPS- stimulated MC^{FosB-} mast cells is at least partly mediated by reduced Mir155hg signaling resulting from FosB ablation. Intriguingly, PI3K has been associated with several other pathways mediating mast cell functions, including G protein-coupled receptor activation in response to adenosine[102] and complement component C3a[103], as well as SCF-mediated mast cell migration[104]. Therefore,

ΔFOSB's enhancement of Mir155hg expression may broadly modulate mast cell responses across different contexts. Future studies should assess this possibility to understand the full scope of ΔFOSB's regulatory influence on mast cell activity.

CLCF1 is a gene that encodes a cytokine-like factor involved in various cellular processes. While CLCF1 role in mast cells remains unknown, in osteoclasts it represses the NF-κB signaling pathway[105], which is crucial for pro-inflammatory cytokine production in activated mast cells[106], suggesting that CLCF1 could limit degranulation in mast cells by suppressing NF-κB signaling.

DUSP4 is part of a large family of dual-specificity MAP kinase phosphatases. DUSP4 dephosphorylates various MAPK isoforms, including ERKs, JNK, and p38[107], which are critical for driving mast cell degranulation and cytokine production downstream of FcεRI and TLRs[108]. Therefore, it is plausible that ΔFOSB indirectly limits the release of mast cell mediators by dephosphorylating MAPKs. Intriguingly, GO analyses of CUT&RUN results revealed many terms enriched by ΔFOSB binding associated with MAPK deactivation in stimulated (i.e., GO:0033550, GO:0017017, GO:0033549) and unstimulated BMMCs (i.e., GO:0033550, GO:0017017, and GO:0033549). It was recently shown that inhibition of a different MAPK, MEK1/2, leads to increased metachromatic staining of mast cell granules and expression of granule-localized, proteoglycan-binding proteases, suggesting that MAPK signaling further regulates the content of secretory granules in mast cells[109]. Since MAPK phosphatases are also enriched in unstimulated BMMCs, this could provide an additional explanation for the exacerbated granule number at baseline in MC^{FosB-} BMMCs.

Lastly, three additional genes identified as functional ΔFOSB targets could also potentially modulate mast cell activity, although their specific roles in these cells are yet to be clarified. These genes have been linked to regulatory functions in other immune cells: Trib1, a member of the Tribbles pseudokinase family, is associated with suppressing T cell activation[110] and reducing B-cell immunoglobulin production[111]; Zbtb32, known as the repressor of GATA3, acts as a negative regulator of memory B cell recall responses[112]; and Gpr171, a G-protein coupled receptor, plays a role in inhibiting T cell receptor-mediated

signaling pathways and cellular proliferation[113]. Given these associations, the impact of these genes on mast cell functions warrants further investigation.

Lack of FosB in mast cells exacerbates mast cell-dependent physiological responses to allergy and infection-like stimuli *in vivo*

Using IgE-mediated PSA stimulation *in vivo*, we found that IgE-DNP sensitized MC^{Fosb-} mice, compared to IgE-sensitized WT, showed an exacerbated drop in rectal temperature and release of plasma histamine. PSA-induced hypothermia is a response dependent on mast cells[71] through two primary mechanisms: first, the release of vasoactive mediators such as histamine, which induce vasodilation and increase vascular permeability[114,115]; and second, the secretion of chymases, a group of proteases that activates TRPV1+ sensory neurons which in turn activate the central thermoregulatory neural circuit leading to a rapid reduction in brown adipose tissue thermogenesis[116]. Although we did not measure chymase release, the fact that chymase is stored together with histamine as a presynthesized mediator in mast cell granules[117], and given that MC^{Fosb-} mice demonstrate increased degranulation in mesenteric mast cells—which contain high levels of chymase[118]—it is possible that elevated chymase, in addition to elevated levels of histamine, significantly contributes to this exaggerated response in MC^{Fosb-} mice.

We further assessed *in vivo* responses to infection-like LPS stimulations and found that MC^{Fosb-} mice also show exaggerated hypothermic responses to LPS. A study using mast cell knockout (KO) mice showed that LPS-induced hypothermia, which seems to serve as a strategy to avoid hypoxia in endotoxic shock[119], is dependent on mast cells[72]. This study further indicated that this response might be partly mediated by TNF-alpha derived from brain-resident mast cells, as mast cell KO mice showed reduced central, but not peripheral, increases in TNF-alpha in response to LPS, in addition to blunted hypothermic responses. Interestingly, more recent studies have identified that the hypothermic versus hyperthermic responses to LPS are mediated by a subsection of the dorsomedial hypothalamus[120]. Mast cells accumulate in the hypothalamus, and our study found that MC^{Fosb} mice have increased LPS-induced *tnf-alpha* expression in the hypothalamus compared to WT controls. Together,

these findings suggest that FosB in mast cells may play a role in mitigating LPS-induced hypothermia by regulating the release of TNF-alpha in the brain.

Conclusions

In summary, our research unveils a key role of FosB in regulating mast cell responses, highlighting how inhibiting its expression can exaggerate physiological reactions to both allergenic and infection-related stimuli. By exploring the transcriptional landscape modulated by FosB, particularly through ΔFOSB, we have identified potential molecular targets that could refine our understanding and treatment of mast cell disorders. Further, considering recent advances in ΔFOSB research that suggest targeting ΔFOSB in a tissue- or cell-specific manner could be achieved by targeting distinct ΔFOSB isoforms or ΔFOSB-containing multiprotein complexes[90], this approach emerges as an attractive therapeutic option to explore for disorders associated with exaggerated mast cell activity. Future studies should further investigate these findings to develop more effective strategies for managing diseases involving mast cell dysregulation, potentially leveraging ΔFOSB as a novel therapeutic avenue.

Methods

Animals. All procedures involving animals were conducted in strict accordance with the ethical guidelines set by the Michigan State University Animal Care Committee. The study utilized in-house bred mice from a cross between MCPT5-$^{Cre/+}$ mice (kindly provided by Dr. Soman Abraham, Duke University, developed by Dr. Axel Roers[121]) and floxed FosB mice generated by Eric Nestler's lab[122]. To generate experimental cohorts, MCPT5-$^{Cre/+}$ homozygous for the floxed fosB allele were crossed with MCPT5-$^{+/+}$ mice also homozygous for the floxed fosB allele. This breeding strategy yielded approximately 50% of mast cell-specific FosB-knockout mice (MCPT5-$^{Cre/+}$; FosB$^{lox/lox}$, referred to as MC^{FosB-}), with the remaining 50% serving as littermate controls (MCPT5$^{+/+}$; FosB$^{lox/lox}$, referred to as WT). Genotyping was performed using standard PCR with specific primers: Mcpt5^{-Cre} Forward 5'-ACAGTGGTATTCCCGGGGAGTGT, Mcpt5^{-Cre} Reverse 5'-GTCAGTGCGTTCAAAGGCCA, and

FosB loxPu sequence 5'-GCTGAA GGAGATGGGTAA CAG-3'. All animals were housed in same-sex groups of 3-4 per cage, with environmental enrichment including Nestlet and Bed-r'Nest® bedding, maintained at 20–23°C in a controlled 12 h light/dark cycle (lights on 6:00am), and provided *ad libitum* access to food and water. For this study, only males were used based on previously observed sex differences in mast cell reactivity and mediator release[18].

Generation of bone marrow derived mast cells (BMMCs). Bone marrow progenitor cells were harvested from the femurs of 6-8-week-old male WT and MC^{FosB-} mice. Following established protocols[18,55], the isolated cells were cultured in a controlled environment at 37°C with 5% CO2. The cultures were maintained in 175 cm^2 flasks filled with 70 mL of complete medium, which consisted of RPMI 1640 (containing L-glutamine), supplemented with 10% heat-inactivated fetal bovine serum (FBS), 1x MEM non-essential amino acids, 10 mmol/L HEPES buffer, 1 mmol/L sodium pyruvate, 100 U/mL penicillin, and 100 µg/mL streptomycin. Additionally, the medium was enriched with recombinant murine interleukin-3 (IL-3; 5 ng/mL) and stem cell factor (SCF; 5 ng/mL) from R&D Systems, Minneapolis, MN. Non-adherent cells were gently transferred to fresh complete medium every 4-5 days. 6 weeks later, purity of mast cell population (>98%) was confirmed using 0.5% toluidine blue staining at pH 0.5 and flow cytometry analysis (BD LSR II) using fluorescently labeled c-kit (BioLegend, San Diego, Calif) and high-affinity IgE receptor (FcεRI) antibodies (eBioscience, San Diego, Calif).

BMMC stimulations. For IgE-mediated FcεRI crosslinking, BMMCs were sensitized overnight with 0.5 µg/mL mouse monoclonal anti-DNP IgE (SPE-7, Sigma-Aldrich). After sensitization, the media was replaced with fresh complete medium and cells were transferred to a 12-well plate at a density of 2 × 10^6 cells per well in 1 mL. Following a one-hour acclimation period at 37°C and 5% CO2, either vehicle or 15 ng/mL DNP-HSA (Sigma-Aldrich) was added to each well. Cell pellets and supernatants were collected and immediately flash frozen one hour later for pellet RNA expression measurements and supernatant analyses and after four hours for pellet protein measurements. For lipopolysaccharides (LPS) stimulation, BMMCs were transferred to a 12-well plate with 2 ×

10^6 cells per well in 1 mL of fresh complete medium. After one hour of incubation at 37°C and 5% CO2, the cells were treated with either vehicle or 500 ng/mL of LPS from Escherichia coli O55:B5 (Sigma-Aldrich). Pellets and supernatants were collected and immediately flash frozen at one hour for pellet RNA expression and supernatant analyses, and at six and twenty-four hours for additional supernatant analyses.

RNA expression analysis: BMMCs: pellets collected one hour after stimulations were homogenized using Trizol (Invitrogen), and total RNA was extracted using the RNAeasy MicroKit (Qiagen #74004). The integrity and concentration of the RNA were assessed using the Nanodrop™ 8000 Spectrophotometer. Subsequently, 200 µg of RNA was converted to cDNA using the Applied Biosystems™ High-Capacity cDNA Reverse Transcription Kit (#4368814). The resulting cDNA was diluted 1:200. Quantitative polymerase chain reaction (qPCR) was then employed to analyze changes in *FosB*, *ΔFosB* gene expressions. For primer pairs information, please refer to **Table 1**. The qPCR reaction mixture consisted of 10 µL PowerSYBR Green PCR Master Mix (Applied Biosystems; #436759), 2 µL each of forward and reverse primers and water, and 4 µL cDNA template per well. The qPCR program proceeded as follows: an initial heating at 95 °C for 10 minutes (Step 1), followed by 50 cycles at 95 °C for 15 seconds, 60 °C for 15 seconds, and 72 °C for 15 seconds (Step 2), and a final step at 95 °C for 15 seconds and 60 °C for 15 seconds (Step 3). Each sample was run in duplicates, and the analysis was conducted using the ΔΔC(t) method[123], with Glyceraldehyde-3-phosphate dehydrogenase (GAPDH) serving as the reference gene for normalization. Hypothalamus: HyFollowing behavior assessment in the elevated plus maze, animals were euthanized via cervical dislocation. Hypothalamic tissue (bregma ~0.05-1.05) was promptly excised using a 2 mm diameter punch tool and flash frozen using dry ice. The protocols for RNA extraction, cDNA synthesis, and qPCR were identical to those used for BMMCs, except the primers targeted *tnf-alpha* expression (table 1).

Table 1.

Transcript of interest	**Forward**	**Reverse**
fosB	5'-GTGAGAGATTTGCCAGGGTC-3'	5'- AGAGAGAAGCCGTCAGGTTG-3'

ΔfosB	5'-AGGCAGAGCTGGAGTCGGAGAT-3'	5'-GCCGAGGACTTGAACTTCACTCC-3'
gapdh	5'-AGGTCGGTGTGAACGGATTTG-3'	5'-TGTAGACAATGTAGTTGAGGTCA-3'
tnf alpha	5'-GATCTCAAAGACAACCAACATGTG-3'	5'-CTCCAGCTGGAAGACTCCTCCCAG-3'

Western blots in BMMC pellets: Frozen BMMC and LAD2 pellets were resuspended in 1.5x Laemmli buffer and homogenized through repeated pipetting. 10 µL of each sample was loaded onto a 4-15% SDS-PAGE gel and electrophoresed at approximately 70V for about two hours. Proteins were subsequently transferred to 0.2 µm PVDF Transfer Membranes (Thermo Scientific) at 60V for around 35 minutes. The membranes were incubated overnight with a rabbit anti-FosB antibody (2251; 1:500 dilution; Cell Signaling Technology), which recognizes both FOSB and ΔFOSB, in 5% BSA at 4°C. Following the primary antibody incubation, membranes were washed and incubated with an HRP-conjugated anti-rabbit secondary antibody (PI-1000; 1:40,000 dilution; Vector Laboratories). Protein signals were detected on film and quantified using ImageJ software. After signal detection, membranes were treated with stripping buffer for 30 minutes and subsequently re-probed with a rabbit anti-GAPDH primary antibody (14C10; 1:20,000 dilution; Cell Signaling Technology) followed by the same HRP-conjugated secondary antibody. Protein quantification values were normalized to total protein content, as detected by Swift Membrane Stain (G-Biosciences).

Histamine and IL-6 ELISAS: Histamine levels in BMMC supernatants, BMMC lysates, and plasma were quantified using a competitive histamine ELISA kit (EA31, Oxford Biomedical Research), strictly adhering to the manufacturer's instructions. IL-6 levels in the supernatant and plasma were determined using a high sensitivity IL-6 ELISA Kit (BMS603HS, Invitrogen) following the manufacturer's instructions. All assays were conducted in duplicates to maintain consistency and reliability in the results.

Intracellular calcium mobilization: On the day of the experiment, cells were washed and resuspended in calcium assay buffer. Intracellular calcium changes in response to stimuli were detected using the Fluo 4 NW Calcium Assay Kit (Thermo Fisher Scientific), following the manufacturer's guidelines. Briefly, cells were incubated at 37°C for 30 minutes with Fluo

4 NW, a fluorescent Ca2+ indicator, in the presence of probenecid to prevent dye efflux. This was followed by a 30-minute incubation at room temperature to allow for complete dye loading. For the measurement of calcium flux, IgE-sensitized cells were stimulated with 0.1 µg/mL DNP/HSA, and unsensitized cells were treated with 0.1 mM A23187. Fluorescence changes were monitored using the FDSS/µCELL kinetic plate reader (Hamamatsu, Japan) at an excitation wavelength of 480 nm and an emission wavelength of 540 nm. This setup provided a dynamic assessment of the cellular response to the added stimuli.

Electron microscopy: BMMC pellets were fixed with 2.5% glutaraldehyde in phosphate buffer (Electron Microscopy). Samples were post-fixed for 1 h in 1% osmium tetroxide/0.1 M sodium phosphate buffer, dehydrated through a graded series of acetones, and embedded in Spurr epoxy resin. Using a diamond knife, 70-nm sections were cut and mounted on 200-mesh copper grids, then stained with 4% aqueous uranyl acetate for 30 min and Reynolds' lead citrate for 14min. Samples were observed using a JEOLL 1400 Flash Transmission Electron Microscope operated at 100kV (Japan Electron Optics Laboratory, Japan). The images were taken at magnifications of 500x and 3000x. A blind observer analyzed these images using ImageJ software to quantify whole cell degranulation status and the number of vesicles per cell, respectively.

Assessment of tissue mast cell numbers and activation status: Small intestinal mesentery windows from WT and MC^{Fosb-} mice at baseline or after passive systemic anaphylaxis or LPS challenges were whole mounted on glass slides, fixed with Carnoy's fixative, and stained with toluidine blue (Sigma-Aldrich, St Louis, Mo) for 30 min, as previously described[55]. Toluidine blue–stained mast cells were counted in 4 nonoverlapping microscopic fields at a magnification of 10x. Each field contained tissue sections that filled the entire high-power field. Mesentery mast cells were counted and scored as inactive (dense staining, non-degranulating) or active (low staining density, granules can be seen outside the cell) by a blind observer using ImageJ in at least 4 mesenteric windows per mouse/treatment. The average number and active/inactive ratio per high-power field was then calculated within each genotype.

Behavior tests: All behavioral tests were performed under red light conditions between 1 and 5 pm (7-11h after lights on) one hour after habituation to the testing room. Open Field Test: Mice were placed at the center of a 38 x 38 cm arena and allowed to explore freely for 3 minutes. The velocity and total distance traveled by each mouse was automatically recorded and quantified using Anymaze software (CleverSys). Elevated Plus Maze: 24h after LPS administration, mice were placed in the center of the maze with the body oriented parallel to the open arms and allowed to freely explore for 5 minutes. The session was video recorded and the Anymaze software (CleverSys) was used to quantify the time spent in both the open and closed arms, as well as the distance traveled during the test.

***In vivo* passive systemic anaphylaxis**: Eight-week-old WT and MC^{fosB-} mice were sensitized with an intraperitoneal injection of 5 µg of anti-DNP IgE (SPE-7, Sigma-Aldrich) in 100 µL of sterile saline. 24h later, the mice were challenged with an intraperitoneal injection of 50 µg of DNP-HSA (Sigma-Aldrich) in 100 µL of saline. Rectal temperatures were recorded right before DNP-HAS injection and every 5 minutes for up to 25 minutes following the DNP challenge using a TH-5 Thermalert thermometer (Physitemp, Clifton, NJ), after which animals were euthanized for tissue collection.

***In vivo* LPS challenge:** Eight-week-old WT and MC^{fosB-} mice were were challenged with an intraperitoneal injection of 1mg/Kg of LPS from Escherichia coli O55:B5 (Sigma-Aldrich) in µL of saline. Rectal temperatures were recorded immediately before the LPS injection and subsequently every 60 minutes for up to 360 minutes using a TH-5 Thermalert thermometer (Physitemp, Clifton, NJ). After the final temperature measurement at 360 minutes, the animals were euthanized for tissue collection. Throughout this period, the mice were closely monitored, and clinical symptoms were assessed and recorded every 60 minutes. The symptoms included reduced activity/alertness, hunched posture, increased respiration rate or labored breathing, ruffled fur, tremors, and inability to move after prodding or to right itself. The overall clinical score for each individual was calculated based on the number of symptoms present, ranging from 0 (no symptoms) to 6 (all symptoms present).

CUT&RUN: BMMC samples of IgE-sensitized BMMC were incubated with either vehicle or DNP in a 12-well plate for 60 minutes as described above. Following incubation, the samples

were centrifuged, and the supernatants were carefully removed. The remaining cell pellets, containing approximately 1x10^6 cells per sample, were immediately frozen in dry ice. Subsequent procedures including Cleavage Under Targets and Release Using Nuclease (CUT&RUN), library preparation, and sequencing were conducted following previously described methods[52,124] and are thoroughly described in **supplementary materials**. For CUT&RUN bioinformatics, peaks were called with MACS2[79] (v.2.2.6)and filtered through Irreproducible Discovery Rate (v.2.0.4.2)[80]. Irreproducible Discovery Rate output for each group was combined with Bedtools (v.2.29.2)[125] for further analysis. ChIPseeker (v.1.22.1) [126]was used to annotate peaks in R (v.3.6.1; RStudio). Venn diagram and motif analyses were carried out using HOMER (v.4.9)[83].

Statistical analyses and figures: All statistical analyses and graphical representations, except those pertaining to CUT&RUN experiments, were performed using GraphPad Prism 9 software. We adopted an alpha level of 0.05 to determine statistical significance. One-tailed T-tests were employed to compare two conditions across all experiments (e.g., treatment effects within a genotype or differences between genotypes in the absence of treatment). Two-way ANOVAs were utilized for experiments assessing the interaction of genotype with another variable (e.g., genotype x treatment). For experiments involving calcium imaging and *in vivo* assessments of rectal temperature and clinical symptoms, repeated measures ANOVAs (genotype x time) were applied. Following significant two-way ANOVA outcomes, post-hoc comparisons between groups were conducted using Fisher's LSD test. Additionally, effect sizes were quantified using R^2 for statistically significant comparisons. All diagrams presented in the figures, including the graphical abstract, were created using BioRender™ software.

<u>Declaration of Competing Interest</u>

The authors declare that they have no known competing financial interests or personal relationships that could have appeared to influence the work reported in this paper.

<u>Acknowledgements</u>

We thank Arnold S. Kirshenbaum, MD, for the donation of the LAD2 cells used in this study, Alicia Withrow and the Center for Advanced Microscopy at Michigan State University for their electron microscopy contributions, and Ken Moon for their excellence technical assistance. This work was supported by a Brain and Behavior Research Foundation 2019 NARSAD Young Investigator Award to NDW; R01 HD072968 to AJM, AJR; and R01 AI168014 to AJM, AJR.

References

1. Tauber, M. *et al.* Landscape of mast cell populations across organs in mice and humans. *J Exp Med* **220**, e20230570 (2023).
2. Kunder, C. A., St John, A. L. & Abraham, S. N. Mast cell modulation of the vascular and lymphatic endothelium. *Blood* **118**, 5383–5393 (2011).
3. Agier, J., Pastwińska, J. & Brzezińska-Błaszczyk, E. An overview of mast cell pattern recognition receptors. *Inflamm Res* **67**, 737–746 (2018).
4. Nakamura, Y. *et al.* Staphylococcus δ-toxin induces allergic skin disease by activating mast cells. *Nature* **503**, 397–401 (2013).
5. Singh, T. S. K., Lee, S., Kim, H.-H., Choi, J. K. & Kim, S.-H. Perfluorooctanoic acid induces mast cell-mediated allergic inflammation by the release of histamine and inflammatory mediators. *Toxicol Lett* **210**, 64–70 (2012).
6. Baram, D. *et al.* Human Mast Cells Release Metalloproteinase-9 on Contact with Activated T Cells: Juxtacrine Regulation by TNF-α1. *The Journal of Immunology* **167**, 4008–4016 (2001).
7. Carroll-Portillo, A. *et al.* Mast cells and dendritic cells form synapses that facilitate antigen transfer for T cell activation. *J Cell Biol* **210**, 851–864 (2015).
8. Rivera, J. & Gilfillan, A. M. Molecular regulation of mast cell activation. *Journal of Allergy and Clinical Immunology* **117**, 1214–1225 (2006).
9. Kalesnikoff, J. *et al.* Monomeric IgE Stimulates Signaling Pathways in Mast Cells that Lead to Cytokine Production and Cell Survival. *Immunity* **14**, 801–811 (2001).
10. Hu, Z.-Q., Zhao, W.-H. & Shimamura, T. Regulation of Mast Cell Development by Inflammatory Factors. *Current Medicinal Chemistry* **14**, 3044–3050.
11. Xu, H. *et al.* Neurotransmitter and neuropeptide regulation of mast cell function: a systematic review. *Journal of Neuroinflammation* **17**, 356 (2020).

12. Alim, M. A. *et al.* Glutamate triggers the expression of functional ionotropic and metabotropic glutamate receptors in mast cells. *Cell Mol Immunol* **18**, 2383–2392 (2021).

13. Cao, J. *et al.* Human mast cells express corticotropin-releasing hormone (CRH) receptors and CRH leads to selective secretion of vascular endothelial growth factor. *J Immunol* **174**, 7665–7675 (2005).

14. Ayyadurai, S. *et al.* Frontline Science: Corticotropin-releasing factor receptor subtype 1 is a critical modulator of mast cell degranulation and stress-induced pathophysiology. *Journal of Leukocyte Biology* **102**, 1299–1312 (2017).

15. Siebler, T. *et al.* Thyroid status affects number and localization of thyroid hormone receptor expressing mast cells in bone marrow. *Bone* **30**, 259–266 (2002).

16. Aldan, J. T. *et al.* Insulin-induced lipid body accumulation is accompanied by lipid remodelling in model mast cells. *Adipocyte* **8**, 265–279 (2019).

17. Zierau, O., Zenclussen, A. C. & Jensen, F. Role of female sex hormones, estradiol and progesterone, in mast cell behavior. *Front Immunol* **3**, 169 (2012).

18. Mackey, E. *et al.* Perinatal androgens organize sex differences in mast cells and attenuate anaphylaxis severity into adulthood. *Proceedings of the National Academy of Sciences* **117**, 23751–23761 (2020).

19. Maldonado, M. D., Gutiérrez-Pérez, M. C., Flores, J. A. & Ales, E. Melatonin reduces exo-endocytosis in mast cells, making it a useful therapeutic tool in inflammatory diseases. *Annals of Allergy, Asthma & Immunology* **131**, 670–672 (2023).

20. Mukai, K., Tsai, M., Saito, H. & Galli, S. J. Mast cells as sources of cytokines, chemokines, and growth factors. *Immunol Rev* **282**, 121–150 (2018).

21. Gulliksson, M., Palmberg, L., Nilsson, G., Ahlstedt, S. & Kumlin, M. Release of prostaglandin D2 and leukotriene C4 in response to hyperosmolar stimulation of mast cells. *Allergy* **61**, 1473–1479 (2006).

22. Nautiyal, K. M. *et al.* Serotonin of mast cell origin contributes to hippocampal function. *Eur J Neurosci* **36**, 2347–2359 (2012).

23. Borriello, F., Iannone, R. & Marone, G. Histamine Release from Mast Cells and Basophils. *Handb Exp Pharmacol* **241**, 121–139 (2017).

24. Rönnberg, E., Calounova, G. & Pejler, G. Mast cells express tyrosine hydroxylase and store dopamine in a serglycin-dependent manner. *Biol Chem* **393**, 107–112 (2012).

25. Wang, L. *et al.* ATP Release from Mast Cells by Physical Stimulation: A Putative Early Step in Activation of Acupuncture Points. *Evid Based Complement Alternat Med* **2013**, 350949 (2013).

26. Shaik-Dasthagirisaheb, Y. B. *et al.* Vascular endothelial growth factor (VEGF), mast cells and inflammation. *Int J Immunopathol Pharmacol* **26**, 327–335 (2013).

27. Leon, A. *et al.* Mast cells synthesize, store, and release nerve growth factor. *Proc Natl Acad Sci U S A* **91**, 3739–3743 (1994).

28. Gülen, T. & Akin, C. Anaphylaxis and Mast Cell Disorders. *Immunology and Allergy Clinics* **42**, 45–63 (2022).

29. Guan, L. C., Dong, X. & Green, D. P. Roles of mast cells and their interactions with the trigeminal nerve in migraine headache. *Mol Pain* **19**, 17448069231181358 (2023).

30. Conti, P. *et al.* Progression in migraine: Role of mast cells and pro-inflammatory and anti-inflammatory cytokines. *European Journal of Pharmacology* **844**, 87–94 (2019).

31. Hamilton, M. J., Frei, S. M. & Stevens, R. L. The Multifaceted Mast Cell in Inflammatory Bowel Disease. *Inflamm Bowel Dis* **20**, 2364–2378 (2014).

32. McClain, J. L. *et al.* Histamine-dependent interactions between mast cells, glia, and neurons are altered following early-life adversity in mice and humans. *Am J Physiol Gastrointest Liver Physiol* **319**, G655–G668 (2020).

33. Conti, P. & Kempuraj, D. Important role of mast cells in multiple sclerosis. *Multiple Sclerosis and Related Disorders* **5**, 77–80 (2016).

34. Maruotti, N., Crivellato, E., Cantatore, F. P., Vacca, A. & Ribatti, D. Mast cells in rheumatoid arthritis. *Clin Rheumatol* **26**, 1–4 (2007).

35. Noto, C. N., Hoft, S. G. & DiPaolo, R. J. Mast Cells as Important Regulators in Autoimmunity and Cancer Development. *Front Cell Dev Biol* **9**, 752350 (2021).

36. Varricchi, G. *et al.* Are Mast Cells MASTers in Cancer? *Frontiers in Immunology* **8**, (2017).

37. Sumantri, S. & Rengganis, I. Immunological dysfunction and mast cell activation syndrome in long COVID. *Asia Pac Allergy* **13**, 50–53 (2023).

38. Miller, C. S., Palmer, R. F., Dempsey, T. T., Ashford, N. A. & Afrin, L. B. Mast cell activation may explain many cases of chemical intolerance. *Environ Sci Eur* **33**, 129 (2021).

39. Theoharides, T. C., Kavalioti, M. & Tsilioni, I. Mast Cells, Stress, Fear and Autism Spectrum Disorder. *Int J Mol Sci* **20**, 3611 (2019).

40. Harcha, P. A. *et al.* Mast Cell and Astrocyte Hemichannels and Their Role in Alzheimer's Disease, ALS, and Harmful Stress Conditions. *Int J Mol Sci* **22**, 1924 (2021).

41. Galli, S. J. & Tsai, M. IgE and mast cells in allergic disease. *Nature medicine* **18**, 693.

42. Eagle, A. L. *et al.* Circuit-specific hippocampal ΔFosB underlies resilience to stress-induced social avoidance. *Nat Commun* **11**, 4484 (2020).

43. Nomaru, H. *et al.* Fosb gene products contribute to excitotoxic microglial activation by regulating the expression of complement C5a receptors in microglia. *Glia* **62**, 1284–1298 (2014).

44. McHenry, J. A. *et al.* The Role of ΔFosB in the Medial Preoptic Area: Differential Effects of Mating and Cocaine History. *Behav Neurosci* **130**, 469–478 (2016).

45. Nestler, E. J., Barrot, M. & Self, D. W. DeltaFosB: a sustained molecular switch for addiction. *Proc Natl Acad Sci U S A* **98**, 11042–11046 (2001).

46. Perrotti, L. I. *et al.* Induction of ΔFosB in Reward-Related Brain Structures after Chronic Stress. *J. Neurosci.* **24**, 10594–10602 (2004).

47. Williams, E. S. *et al.* Androgen-Dependent Excitability of Mouse Ventral Hippocampal Afferents to Nucleus Accumbens Underlies Sex-Specific Susceptibility to Stress. *Biological Psychiatry* **87**, 492–501 (2020).

48. Hope, B., Kosofsky, B., Hyman, S. E. & Nestler, E. J. Regulation of immediate early gene expression and AP-1 binding in the rat nucleus accumbens by chronic cocaine. *Proceedings of the National Academy of Sciences* **89**, 5764–5768 (1992).

49. Manning, C. E. *et al.* Hippocampal Subgranular Zone FosB Expression Is Critical for Neurogenesis and Learning. *Neuroscience* **406**, 225–233 (2019).

50. Scholten, J. *et al.* Mast cell-specific Cre/loxP-mediated recombination in vivo. *Transgenic Res* **17**, 307–315 (2008).

51. Ohnishi, Y. N. *et al.* Generation and validation of a floxed FosB mouse line. *bioRxiv* 179309 (2017) doi:10.1101/179309.

52. Yeh, S.-Y. *et al.* Cell Type-Specific Whole-Genome Landscape of ΔFOSB Binding in the Nucleus Accumbens After Chronic Cocaine Exposure. *Biol Psychiatry* **94**, 367–377 (2023).

53. Metzger, H. The receptor with high affinity for IgE. *Immunol Rev* **125**, 37–48 (1992).

54. Turner, H. & Kinet, J. P. Signalling through the high-affinity IgE receptor Fc epsilonRI. *Nature* **402**, B24-30 (1999).

55. D'Costa, S. *et al.* Mast cell corticotropin-releasing factor subtype 2 suppresses mast cell degranulation and limits the severity of anaphylaxis and stress-induced intestinal permeability. *Journal of Allergy and Clinical Immunology* **143**, 1865-1877.e4 (2019).

56. Mackey, E. *et al.* Perinatal androgens organize sex differences in mast cells and attenuate anaphylaxis severity into adulthood. *Proc Natl Acad Sci U S A* **117**, 23751–23761 (2020).

57. Marshall, J. S. Mast-cell responses to pathogens. *Nat Rev Immunol* **4**, 787–799 (2004).

58. Supajatura, V. *et al.* Differential responses of mast cell Toll-like receptors 2 and 4 in allergy and innate immunity. *J Clin Invest* **109**, 1351–1359 (2002).

59. Konopka, Ł., Wierzbicki, M. & Brzezińska-Błaszczyk, E. Lipopolysaccharide from Porphyromonas Gingivalis Stimulates Rat Mast Cells to Cysteinyl Leukotriene Generation and Upregulates Toll-like Receptor −2 and −4 Expression. *Int J Immunopathol Pharmacol* **23**, 803–810 (2010).

60. Orinska, Z. *et al.* TLR3-induced activation of mast cells modulates CD8+ T-cell recruitment. *Blood* **106**, 978–987 (2005).

61. Supajatura, V. *et al.* Protective roles of mast cells against enterobacterial infection are mediated by Toll-like receptor 4. *J Immunol* **167**, 2250–2256 (2001).

62. Sandig, H. & Bulfone-Paus, S. TLR signaling in mast cells: common and unique features. *Front Immunol* **3**, 185 (2012).

63. S. Kirshenbaum, A., Yin, Y., Sundstrom, J. B., Bandara, G. & D. Metcalfe, D. Description and Characterization of a Novel Human Mast Cell Line for Scientific Study. *Int J Mol Sci* **20**, 5520 (2019).

64. McNeil, B. D. *et al.* Identification of a mast cell specific receptor crucial for pseudo-allergic drug reactions. *Nature* **519**, 237–241 (2015).

65. Alim, M. A. *et al.* Glutamate triggers the expression of functional ionotropic and metabotropic glutamate receptors in mast cells. *Cell Mol Immunol* **18**, 2383–2392 (2021).

66. Baumruker, T. *et al.* Activation of mast cells by incorporation of cholesterol into rafts. *Int Immunol* **15**, 1207–1218 (2003).

67. Holowka, D. *et al.* Roles for Ca2+ Mobilization and Its Regulation in Mast Cell Functions. *Frontiers in Immunology* **3**, (2012).

68. Dedkova, E. N., Sigova, A. A. & Zinchenko, V. P. Mechanism of action of calcium ionophores on intact cells: ionophore-resistant cells. *Membr Cell Biol* **13**, 357–368 (2000).

69. Mackey, E. *et al.* Sexual dimorphism in the mast cell transcriptome and the pathophysiological responses to immunological and psychological stress. *Biol Sex Differ* **7**, 60 (2016).

70. Enerbäck, L. & Lundin, P. M. Ultrastructure of mucosal mast cells in normal and compound 48/80-treated rats. *Cell Tissue Res.* **150**, 95–105 (1974).

71. Feyerabend, T. B. *et al.* Cre-mediated cell ablation contests mast cell contribution in models of antibody- and T cell-mediated autoimmunity. *Immunity* **35**, 832–844 (2011).

72. Nautiyal, K. M., McKellar, H., Silverman, A.-J. & Silver, R. Mast cells are necessary for the hypothermic response to LPS-induced sepsis. *American Journal of Physiology - Regulatory, Integrative and Comparative Physiology* **296**, R595 (2009).

73. Romanovsky, A. A. *et al.* Fever and hypothermia in systemic inflammation: recent discoveries and revisions. *Front Biosci* **10**, 2193–2216 (2005).

74. Salazar, A., Gonzalez-Rivera, B. L., Redus, L., Parrott, J. M. & O'Connor, J. C. Indoleamine 2,3-dioxygenase mediates anhedonia and anxiety-like behaviors caused by peripheral lipopolysaccharide immune challenge. *Horm Behav* **62**, 202–209 (2012).

75. Zheng, Z.-H. *et al.* Neuroinflammation induces anxiety- and depressive-like behavior by modulating neuronal plasticity in the basolateral amygdala. *Brain, Behavior, and Immunity* **91**, 505–518 (2021).

76. Dong, H. *et al.* Stabilization of Brain Mast Cells Alleviates LPS-Induced Neuroinflammation by Inhibiting Microglia Activation. *Frontiers in Cellular Neuroscience* **13**, (2019).

77. Wang, Y. *et al.* The Mast Cell Is an Early Activator of Lipopolysaccharide-Induced Neuroinflammation and Blood-Brain Barrier Dysfunction in the Hippocampus. *Mediators of Inflammation* **2020**, e8098439 (2020).

78. Skene, P. J. & Henikoff, S. An efficient targeted nuclease strategy for high-resolution mapping of DNA binding sites. *Elife* **6**, e21856 (2017).

79. Zhang, Y. *et al.* Model-based Analysis of ChIP-Seq (MACS). *Genome Biology* **9**, R137 (2008).

80. Li, Q., Brown, J. B., Huang, H. & Bickel, P. J. Measuring reproducibility of high-throughput experiments. *The Annals of Applied Statistics* **5**, 1752–1779 (2011).

81. Bailey, T. L., Johnson, J., Grant, C. E. & Noble, W. S. The MEME Suite. *Nucleic Acids Research* **43**, W39–W49 (2015).

82. Ramírez, F., Dündar, F., Diehl, S., Grüning, B. A. & Manke, T. deepTools: a flexible platform for exploring deep-sequencing data. *Nucleic Acids Res* **42**, W187–W191 (2014).

83. Heinz, S. *et al.* Simple combinations of lineage-determining transcription factors prime cis-regulatory elements required for macrophage and B cell identities. *Mol Cell* **38**, 576–589 (2010).

84. Mi, H., Muruganujan, A., Casagrande, J. T. & Thomas, P. D. Large-scale gene function analysis with the PANTHER classification system. *Nat Protoc* **8**, 1551–1566 (2013).

85. Hagemann, P. M., Nsiah-Dosu, S., Hundt, J. E., Hartmann, K. & Orinska, Z. Modulation of Mast Cell Reactivity by Lipids: The Neglected Side of Allergic Diseases. *Front. Immunol.* **10**, (2019).

86. Dichlberger, A., Kovanen, P. T. & Schneider, W. J. Mast cells: from lipid droplets to lipid mediators. *Clin Sci (Lond)* **125**, 121–130 (2013).

87. Meghnem, D., Leong, E., Pinelli, M., Marshall, J. S. & Di Cara, F. Peroxisomes Regulate Cellular Free Fatty Acids to Modulate Mast Cell TLR2, TLR4, and IgE-Mediated Activation. *Front. Cell Dev. Biol.* **10**, (2022).

88. DiffBind. *Bioconductor* http://bioconductor.org/packages/DiffBind/.

89. Biethahn, K. *et al.* miRNA-155 controls mast cell activation by regulating the PI3Kγ pathway and anaphylaxis in a mouse model. *Allergy* **69**, 752–762 (2014).

90. Robison, A. J. & Nestler, E. J. ΔFOSB: A Potentially Druggable Master Orchestrator of Activity-Dependent Gene Expression. *ACS Chem Neurosci* **13**, 296–307 (2022).

91. Pardanani, A. Systemic mastocytosis in adults: 2017 update on diagnosis, risk stratification and management. *American Journal of Hematology* **91**, 1146–1159 (2016).

92. Kobayashi, T., Shimabukuro-Demoto, S., Tsutsui, H. & Toyama-Sorimachi, N. Type I interferon limits mast cell–mediated anaphylaxis by controlling secretory granule homeostasis. *PLOS Biology* **17**, e3000530 (2019).

93. Tagen, M. *et al.* Mitochondrial Uncoupling Protein 2 Inhibits Mast Cell Activation and Reduces Histamine Content1. *The Journal of Immunology* **183**, 6313–6319 (2009).

94. Guo, Y. *et al.* Insights into the Characteristics and Functions of Mast Cells in the Gut. *Gastroenterology Insights* **14**, 637–652 (2023).

95. Nautiyal, K. M., Ribeiro, A. C., Pfaff, D. W. & Silver, R. Brain mast cells link the immune system to anxiety-like behavior. *Proc Natl Acad Sci U S A* **105**, 18053–18057 (2008).

96. Chikahisa, S. *et al.* Histamine from Brain Resident MAST Cells Promotes Wakefulness and Modulates Behavioral States. *PLOS ONE* **8**, e78434 (2013).

97. Deiteren, A., De Man, J. G., Pelckmans, P. A. & De Winter, B. Y. Histamine H4 receptors in the gastrointestinal tract. *British Journal of Pharmacology* **172**, 1165–1178 (2015).

98. Pham, L. *et al.* The interplay between mast cells, pineal gland, and circadian rhythm: Links between histamine, melatonin, and inflammatory mediators. *J Pineal Res* **70**, e12699 (2021).

99. Kim, M.-S., Rådinger, M. & Gilfillan, A. M. The multiple roles of phosphoinositide 3-kinase in mast cell biology. *Trends Immunol* **29**, 493–501 (2008).

100. Sly, L. M., Rauh, M. J., Kalesnikoff, J., Song, C. H. & Krystal, G. LPS-Induced Upregulation of SHIP Is Essential for Endotoxin Tolerance. *Immunity* **21**, 227–239 (2004).

101. Hochdörfer, T. *et al.* Activation of the PI3K pathway increases TLR-induced TNF-α and IL-6 but reduces IL-1β production in mast cells. *Cellular Signalling* **23**, 866–875 (2011).

102. Laffargue, M. *et al.* Phosphoinositide 3-kinase gamma is an essential amplifier of mast cell function. *Immunity* **16**, 441–451 (2002).

103. Venkatesha, R. T., Berla Thangam, E., Zaidi, A. K. & Ali, H. Distinct regulation of C3a-induced MCP-1/CCL2 and RANTES/CCL5 production in human mast cells by extracellular signal regulated kinase and PI3 kinase. *Mol Immunol* **42**, 581–587 (2005).

104. Kim, M.-S., Kuehn, H. S., Metcalfe, D. D. & Gilfillan, A. M. Activation and function of the mTORC1 pathway in mast cells. *J Immunol* **180**, 4586–4595 (2008).

105. Yokota, S. *et al.* Cardiotrophin Like Cytokine Factor 1 (CLCF1) alleviates bone loss in osteoporosis mouse models by suppressing osteoclast differentiation through activating interferon signaling and repressing the nuclear factor-κB signaling pathway. *Bone* **153**, 116140 (2021).

106. Kalesnikoff, J. *et al.* SHIP Negatively Regulates IgE + Antigen-Induced IL-6 Production in Mast Cells by Inhibiting NF-κB Activity1. *The Journal of Immunology* **168**, 4737–4746 (2002).

107. Bermudez, O., Pagès, G. & Gimond, C. The dual-specificity MAP kinase phosphatases: critical roles in development and cancer. *Am J Physiol Cell Physiol* **299**, C189-202 (2010).

108. Sandig, H. & Bulfone-Paus, S. TLR signaling in mast cells: common and unique features. *Front Immunol* **3**, 185 (2012).

109. Hu Frisk, J. M., Kjellén, L., Melo, F. R., Öhrvik, H. & Pejler, G. Mitogen-Activated Protein Kinase Signaling Regulates Proteoglycan Composition of Mast Cell Secretory Granules. *Front. Immunol.* **9**, (2018).

110. Rome, K. S. *et al.* Trib1 regulates T cell differentiation during chronic infection by restraining the effector program. *J Exp Med* **217**, e20190888 (2020).

111. Simoni, L. *et al.* Trib1 Is Overexpressed in Systemic Lupus Erythematosus, While It Regulates Immunoglobulin Production in Murine B Cells. *Front Immunol* **9**, 373 (2018).

112. Jash, A. *et al.* ZBTB32 Restricts the Duration of Memory B Cell Recall Responses. *J Immunol* **197**, 1159–1168 (2016).

113. Fujiwara, Y. *et al.* The GPR171 pathway suppresses T cell activation and limits antitumor immunity. *Nat Commun* **12**, 5857 (2021).

114. Makabe-Kobayashi, Y. *et al.* The control effect of histamine on body temperature and respiratory function in IgE-dependent systemic anaphylaxis. *J Allergy Clin Immunol* **110**, 298–303 (2002).

115. Kanjarawi, R. *et al.* Regulatory CD4+Foxp3+ T Cells Control the Severity of Anaphylaxis. *PLoS One* **8**, e69183 (2013).

116. Bao, C. *et al.* A mast cell–thermoregulatory neuron circuit axis regulates hypothermia in anaphylaxis. *Science Immunology* **8**, eadc9417 (2023).

117. Pejler, G., Rönnberg, E., Waern, I. & Wernersson, S. Mast cell proteases: multifaceted regulators of inflammatory disease. *Blood* **115**, 4981–4990 (2010).

118. Pejler, G. Novel Insight into the in vivo Function of Mast Cell Chymase: Lessons from Knockouts and Inhibitors. *J Innate Immun* **12**, 357–372 (2020).

119. Corrigan, J. J., Fonseca, M. T., Flatow, E. A., Lewis, K. & Steiner, A. A. Hypometabolism and hypothermia in the rat model of endotoxic shock: independence of circulatory hypoxia. *J Physiol* **592**, 3901–3916 (2014).

120. Wanner, S. P. *et al.* Cold-Induced Thermogenesis and Inflammation-Associated Cold-Seeking Behavior Are Represented by Different Dorsomedial Hypothalamic Sites: A Three-Dimensional Functional Topography Study in Conscious Rats. *J. Neurosci.* **37**, 6956–6971 (2017).

121. Scholten, J. *et al.* Mast cell-specific Cre/loxP-mediated recombination in vivo. *Transgenic Res* **17**, 307–315 (2008).

122. Ohnishi, Y. N. *et al. Generation and Validation of a Floxed FosB Mouse Line*. 179309 https://www.biorxiv.org/content/10.1101/179309v1 (2017) doi:10.1101/179309.

123. Livak, K. J. & Schmittgen, T. D. Analysis of Relative Gene Expression Data Using Real-Time Quantitative PCR and the 2−ΔΔCT Method. *Methods* **25**, 402–408 (2001).

124. Skene, P. J., Henikoff, J. G. & Henikoff, S. Targeted in situ genome-wide profiling with high efficiency for low cell numbers. *Nat Protoc* **13**, 1006–1019 (2018).

125. Quinlan, A. R. & Hall, I. M. BEDTools: a flexible suite of utilities for comparing genomic features. *Bioinformatics* **26**, 841–842 (2010).

126. Yu, G., Wang, L.-G. & He, Q.-Y. ChIPseeker: an R/Bioconductor package for ChIP peak annotation, comparison and visualization. *Bioinformatics* **31**, 2382–2383 (2015).

Figure legends

Fig. 1. IgE-mediated and LPS stimulations increase fosB gene expression in mast cells progenitors. **A.** Timeline showing BMMC isolation, culture and DNP-mediated IgE-FcεRI crosslinking **. B.** Western blot showing expression of FOSB (50kDa) and ΔFOSB (37 kDa) at baseline and after DNP stimulation in IgE-sensitized BMMCs. **C, D**. T-tests comparing relative expression of *fosb* and *Δfosb* mRNA after DNP stimulation in IgE-sensitized BMMCs. **E, F.** T-tests comparing relative expression of FOSB and ΔFOSB protein after DNP stimulation in IgE-sensitized BMMCs. **G.** Timeline of LPS-mediated BMMC stimulation. **H, I.** T-tests comparing relative expression of *fosb* and *Δfosb* mRNA after LPS stimulation in BMMCs. **J.** Western blot showing C48/80 induced expression of FOSB (50kDa) and ΔFOSB (37 kDa) in human mast cell progenitors LAD2.

Fig. 2. Inhibition of FosB gene expression in mast cells enhances storage capacity, increases sensitivity and histamine release in response to IgE-FcεRI crosslinking, and augments IL-6 release in response to LPS stimulation. A. Timeline of BMMC isolation and culture from WT and MC^{FosB-} mice**. B,C.** Two-way ANOVAs comparing relative expression of *fosb* and *Δfosb* mRNA after DNP stimulation in IgE-sensitized WT and MC^{FosB-} BMMCs. **D.** Western blot showing induction of FOSB (50kDa) and ΔFOSB (37 kDa) expression after IgE-mediated stimulation in WT but not MC^{FosB-} BMMCs. **E.** Two-way ANOVAs comparing histamine release at baseline and after DNP stimulation in IgE-sensitized WT and MC^{FosB-} BMMCs. **F.** T-test comparing histamine content at baseline in WT and MC^{FosB-} BMMCs. **G,H.** Calcium mobilization in WT and MC^{FosB-} BMMCs in response to IgE-mediated and A23187 stimulations. **I.** Two-way ANOVAs comparing IL-6 release at baseline and after 6 or 24h after stimulation with LPS in WT and MC^{FosB-} BMMCs. **J.** T-test showing average vesicle number per cell in WT and MC^{FosB-} BMMCs in images obtained by EM. **K.** Example of EM images used for quantification of vesicle number. **L.** Two-way ANOVA comparing the ratio of highly degranulated vs. total cells in WT and MC^{FosB-} BMMCs. **M.** Example of EM images used for assessment of activation levels in groups of WT and MC^{FosB-} BMMCs.

Fig. 3. Mast cell-specific knockout of FosB exacerbates inflammatory responses in models of systemic anaphylaxis and lipopolysaccharide-induced sepsis. A. Figure depicting WT and MC^{FosB-} mice**. B, C, D, E.** T-tests showing no differences between WT and MC^{FosB-} mice in bodyweight at 6 weeks old, number of mast cells in mesenteric tissues, or locomotor activity in the open field tests as measured by distance and velocity. **F.** Timeline showing passive systemic anaphylaxis experiment. **G.** Two way ANOVA showing PSA-induced hypothermic responses in WT and MC^{FosB-} mice. **H,I.** T-test comparing plasma histamine and active/inactive ratio of mesenteric mast cells 25 minutes after PSA in WT and MC^{FosB-} mice. **J.** Timeline showing LPS-stimulation experiment. **K.** Two way ANOVA showing LPS-induced hypothermic responses in WT and MC^{FosB-} mice. **L,M.** T-test comparing plasma IL-6 and active/inactive ratio of mesenteric mast cells 360 minutes after PSA in WT and MC^{FosB-} mice. **N.** Two-way ANOVA showing time spent in the open vs. closed arms in the elevated plus maze test 24h after injections with vehicle or 1mg/Kg LPS in WT and MC^{FosB-} mice.

Fig. 4. Mapping binding sites of ΔFOSB in unstimulated and stimulated mast cells using CUT&RUN approach. A. Figure depicting experimental design used for ΔFOSB CUT&RUN experiment. **B.** ΔFOSB**-binding peak comparison between stimulated and unstimulated WT BMMCs . C.** Motif analysis of the peaks identified in stimulated and unstimulated WT BMMCs. **D.** Identified genomic regions to which ΔFOSB binds under stimulated conditions in BMMCs. **E,F.** Molecular GO analyses of gene lists corresponding to ΔFOSB binding sites in unstimulated and stimulated WT BMMCs

Fig. 5. Identification of ΔFOSB functional targets in IgE-FcER stimulation in mast cells. A, B. ΔFosb coverage at unstimulated/stimulated peaks in BMMCs. **C.** Diagram depicting strategy used to identify ΔFOSB's functional targets. **D.** Volcano plot illustrating differential binding of ΔFOSB targets in stimulated versus unstimulated BMMCs. **E.** Table of functional targets showing genes with significant changes in expression and ΔFOSB binding in stimulated BMMCs.

Fig. 1.

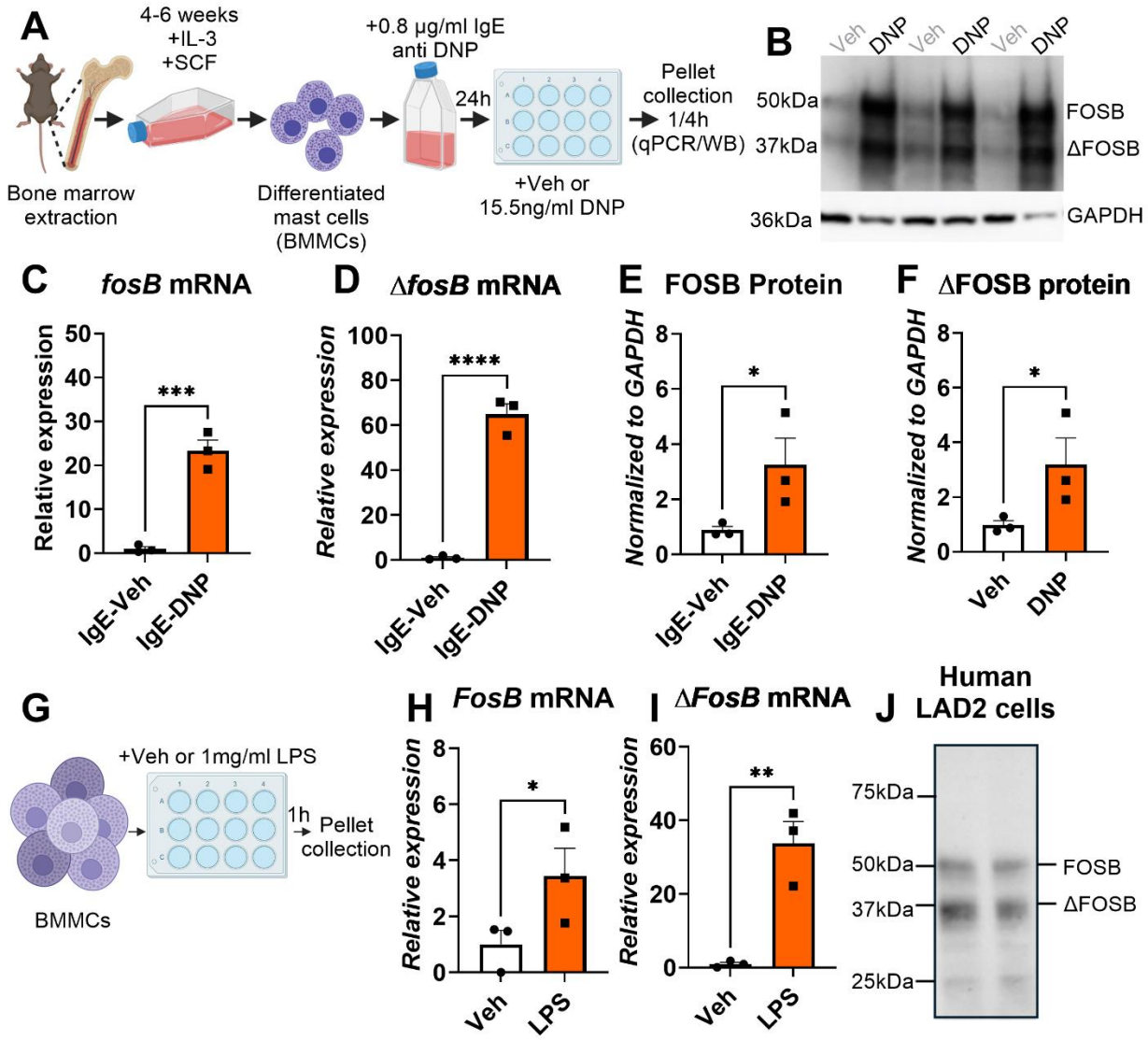
A
4-6 weeks
+IL-3
+SCF
+0.8 µg/ml IgE
anti DNP
24h
Pellet
collection
1/4h
(qPCR/WB)
Bone marrow
extraction
Differentiated
mast cells
(BMMCs)
+Veh or
15.5ng/ml DNP
B
Veh
DNP
Veh
DNP
Veh
DNP
50kDa
37kDa
36kDa
FOSB
ΔFOSB
GAPDH
C
fosB mRNA
Relative expression
***
IgE-Veh
IgE-DNP
D
ΔfosB mRNA
Relative expression
****
IgE-Veh
IgE-DNP
E
FOSB Protein
Normalized to GAPDH
*
IgE-Veh
IgE-DNP
F
ΔFOSB protein
Normalized to GAPDH
*
Veh
DNP
G
+Veh or 1mg/ml LPS
1h
Pellet
collection
BMMCs
H
FosB mRNA
Relative expression
*
Veh
LPS
I
ΔFosB mRNA
Relative expression
**
Veh
LPS
J
Human
LAD2 cells
75kDa
50kDa
37kDa
25kDa
FOSB
ΔFOSB

Fig. 2.

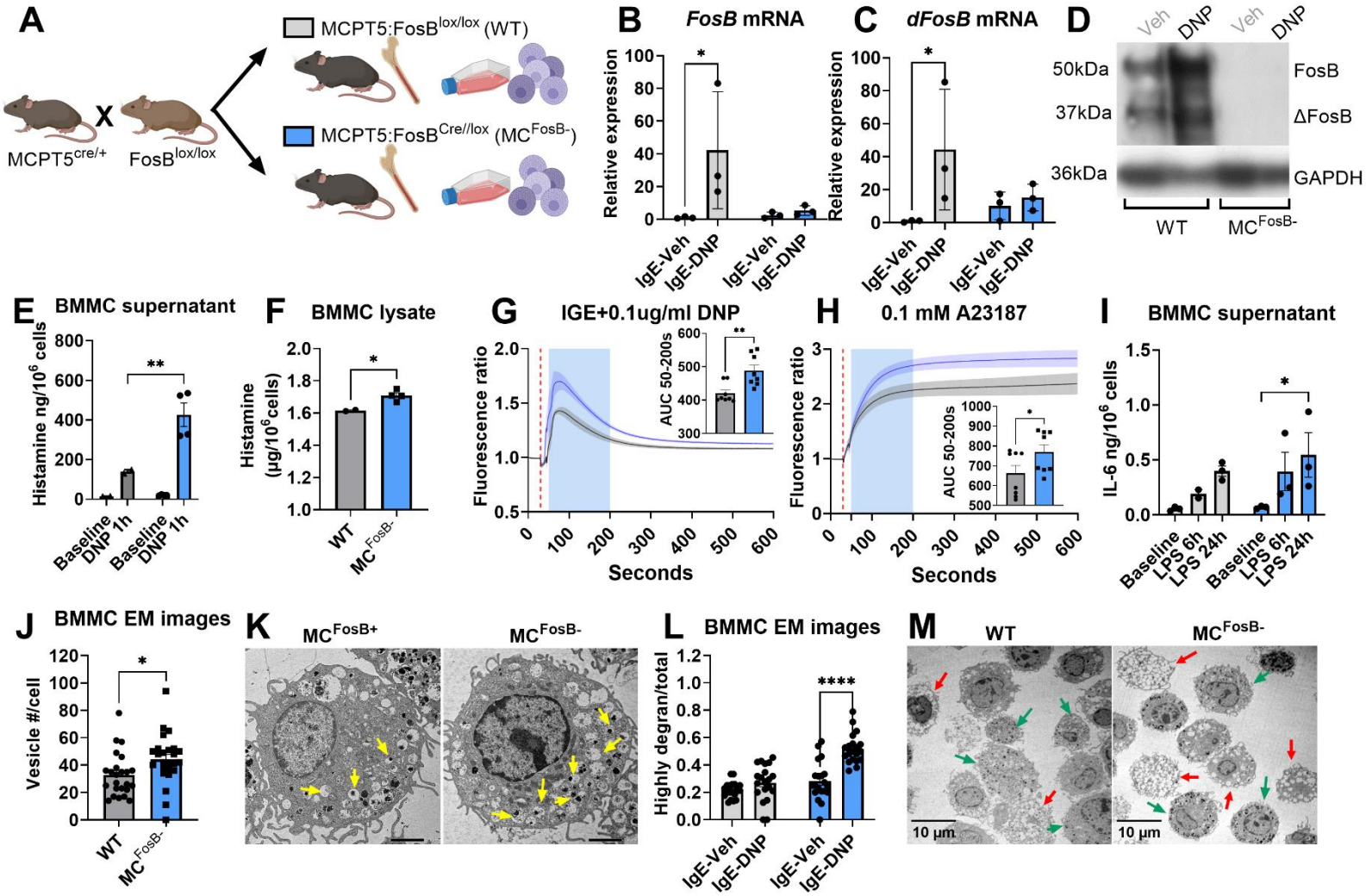
A
MCPT5:FosB lox/lox (WT)
MCPT5:FosB Cre//lox (MC FosB-)
MCPT5 cre/+
FosB lox/lox
B
FosB mRNA
Relative expression
IgE-Veh
IgE-DNP
C
dFosB mRNA
D
Veh
DNP
50kDa
37kDa
36kDa
FosB
ΔFosB
GAPDH
WT
MC FosB-
E
BMMC supernatant
Histamine ng/10^6 cells
Baseline
DNP 1h
F
BMMC lysate
Histamine (µg/10^6 cells)
G
IGE+0.1ug/ml DNP
Fluorescence ratio
AUC 50-200s
Seconds
H
0.1 mM A23187
I
BMMC supernatant
IL-6 ng/10^6 cells
LPS 6h
LPS 24h
J
BMMC EM images
Vesicle #/cell
K
MC FosB+
MC FosB-
L
BMMC EM images
Highly degran/total
M
WT
MC FosB-
10 µm

Fig. 3.

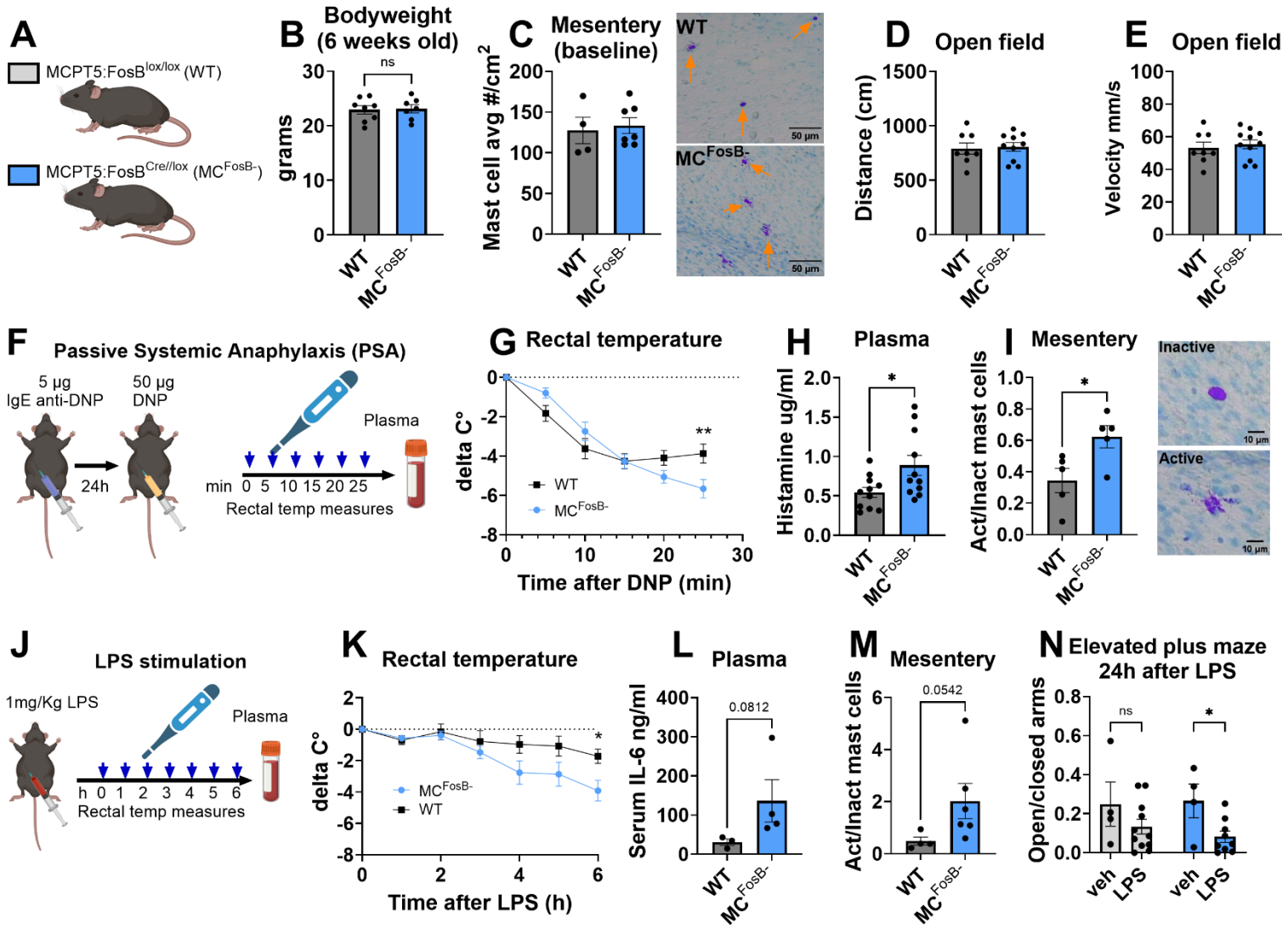
A
MCPT5:FosB lox/lox (WT)
MCPT5:FosB Cre//lox (MC FosB-)
B Bodyweight (6 weeks old)
ns
grams
WT
MC FosB-
C Mesentery (baseline)
Mast cell avg #/cm2
WT
MC FosB-
50 µm
D Open field
Distance (cm)
E Open field
Velocity mm/s
F Passive Systemic Anaphylaxis (PSA)
5 µg IgE anti-DNP
50 µg DNP
24h
Plasma
min 0 5 10 15 20 25
Rectal temp measures
G Rectal temperature
delta C°
Time after DNP (min)
H Plasma
Histamine ug/ml
I Mesentery
Act/Inact mast cells
Inactive
Active
10 µm
J LPS stimulation
1mg/Kg LPS
Plasma
h 0 1 2 3 4 5 6
Rectal temp measures
K Rectal temperature
delta C°
Time after LPS (h)
L Plasma
Serum IL-6 ng/ml
0.0812
M Mesentery
Act/Inact mast cells
0.0542
N Elevated plus maze 24h after LPS
Open/closed arms
ns
veh
LPS

Fig. 4.

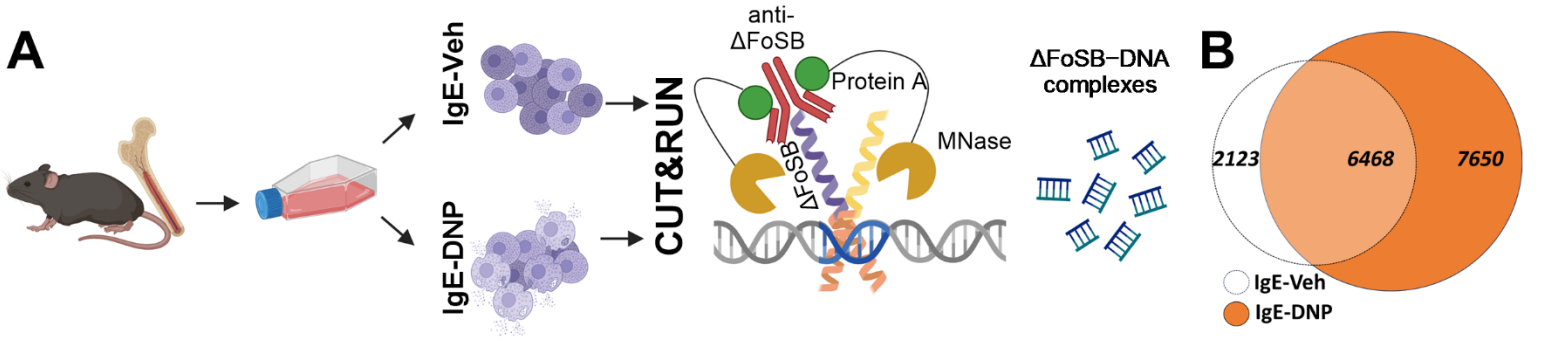

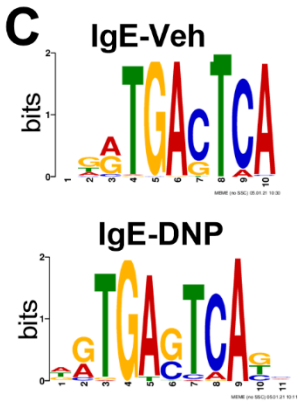

	IgE-Veh	IgE-DNP
# target sequences with motif	8520	14147
% target sequences with motif	98.3	99.4
E-value	1.3×10^{-70}	8.7×10^{-51}

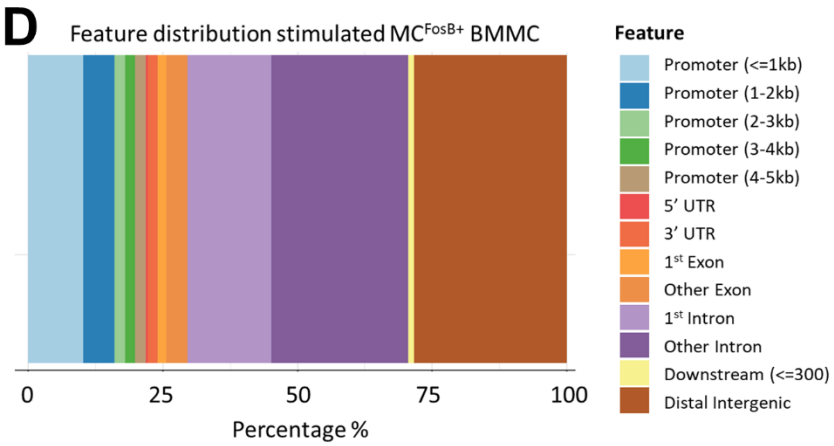

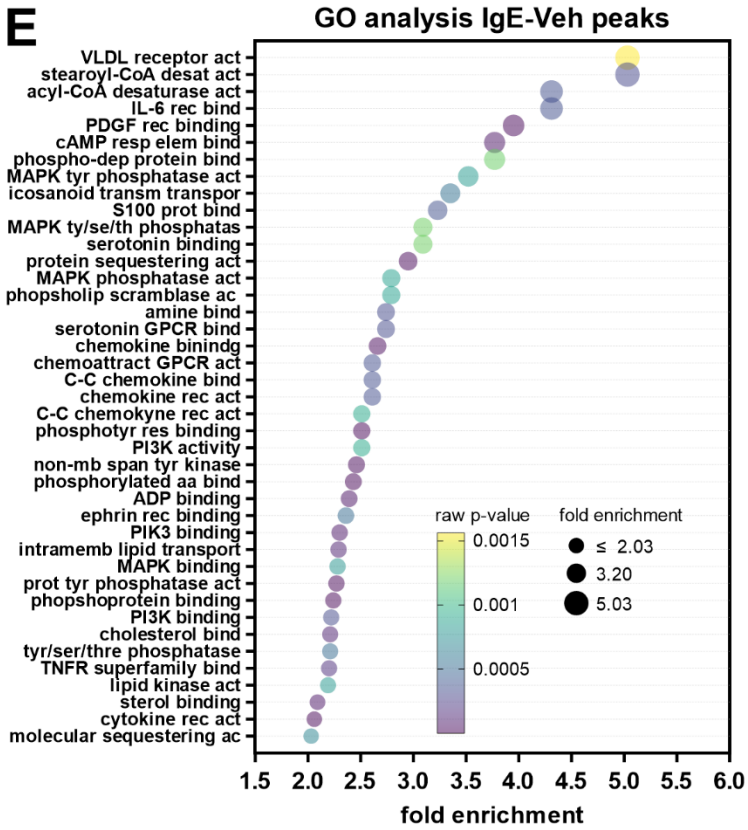

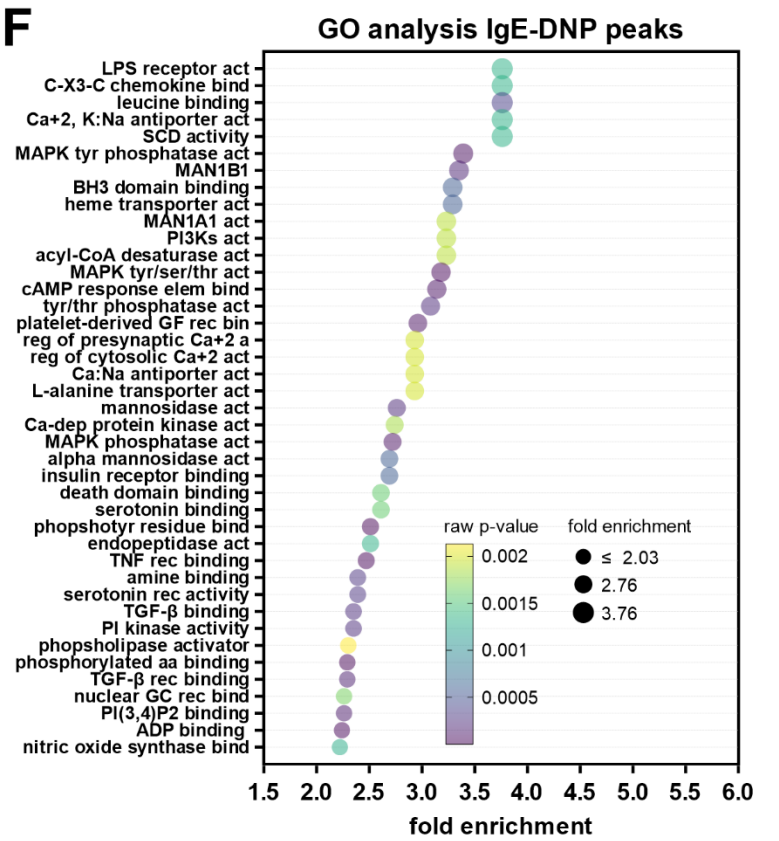

Fig. 5.

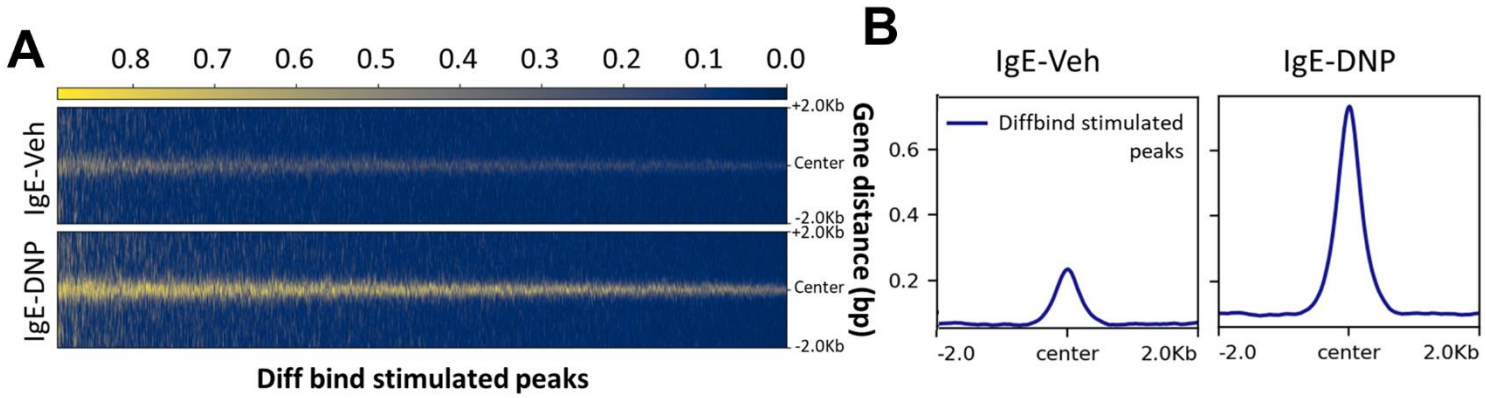

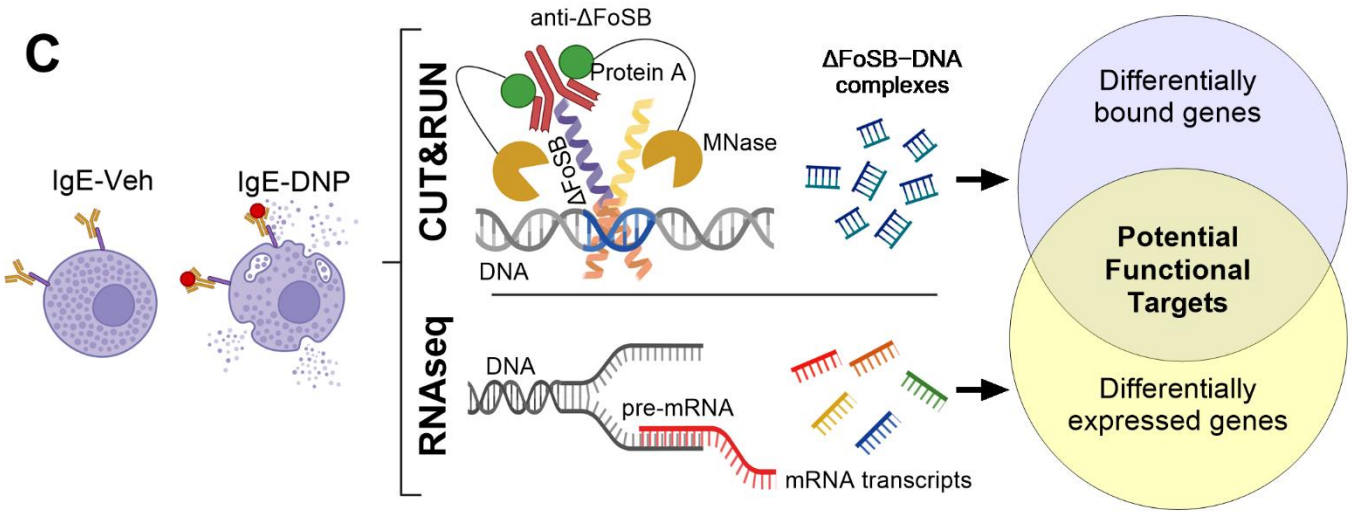

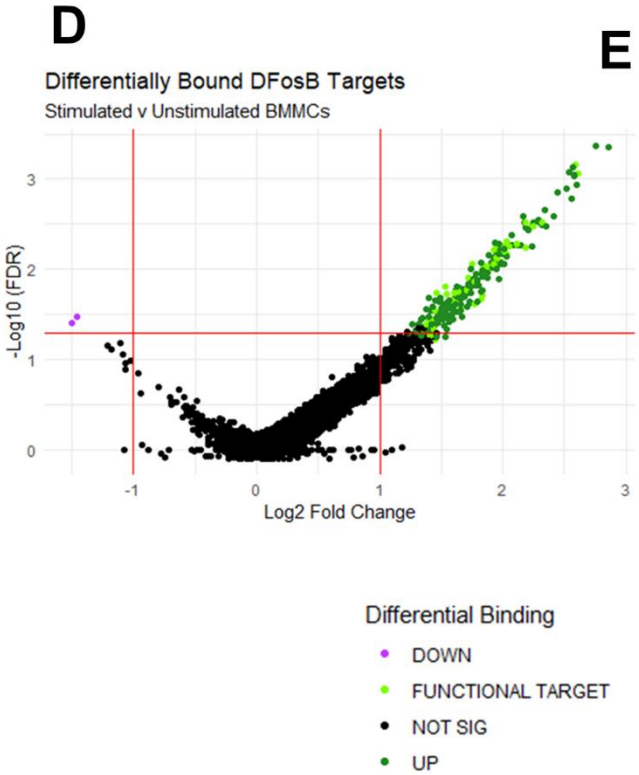

E **Functional targets (>2.0 fold change only)**

Gene	baseMean	log2FoldChange	lfcSE	stat	pvalue	padj (FDR)
Crabp2	163.4730844	9.127640417	1.04771	8.711988	2.99E-18	5.64E-17
Trib1	820.8213085	8.753357833	0.711328	12.30566	8.44E-35	4.19E-33
Phxr4	8.461990811	6.71124572	1.360386	4.93334	8.08E-07	4.88E-06
Zbtb32	9.300362541	4.93839831	1.186183	4.163269	3.14E-05	0.000144
Myo16	8.380220836	4.803069798	1.22929	3.907191	9.34E-05	0.000393
Snai3	7.45197176	4.617452483	1.230792	3.751612	0.000176	0.000699
Plet1	2.632252684	3.979081855	1.601595	2.48445	0.012975	0.032619
Gpr171	14173.6202	3.569991553	0.141243	25.27552	5.9E-141	4E-138
Mir155hg	287.3195096	3.378285136	0.182895	18.47121	3.52E-76	6.25E-74
Clcf1	56.1275272	3.224592454	0.466302	6.915244	4.67E-12	5.22E-11
Tslp	14.52450802	3.166470937	0.658204	4.810776	1.5E-06	8.71E-06
Add2	84.50443644	3.027564163	0.476433	6.35465	2.09E-10	1.99E-09
Dusp2	309.310494	2.978618308	0.194506	15.31376	6.19E-53	6.18E-51
Zfp703	1065.612318	2.788061751	0.174104	16.0138	1.02E-57	1.16E-55
Fhdc1	193.3784311	2.733056878	0.19254	14.19475	9.87E-46	7.78E-44
Sema4b	1867.400219	2.709178054	0.129442	20.92967	2.87E-97	7.92E-95
Dusp4	2627.392276	2.494867115	0.180785	13.80018	2.54E-43	1.84E-41
Sla	14371.67566	2.097046602	0.199141	10.53044	6.25E-26	2.03E-24